VERIFICATION OF AIRWORTHINESS OF A MODIFIED KR-2 AIRCRAFT

A Project

Presented to

The Faculty of the Department of Mechanical and Aerospace Engineering

San Jose State University

In Partial Fulfillment

of the Requirements for the Degree

of Master of Science in Mechanical Engineering

By

Michael Jan Nordin

December 2006

APPROVED FOR THE DEPARTMENT OF
MECHANICAL AND AEROSPACE ENGINEERING

Dr. Nikos J. Mourtos

Dr. Periklis Papadopoulos

Dr. Sean Swei

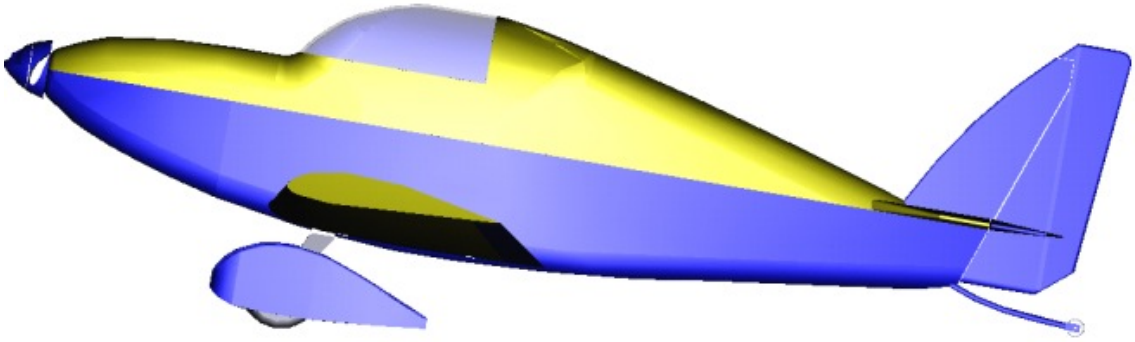

Figure 1: Modified KR-2 CAD Model

I. Abstract

The KR-2 was originally designed by Ken Rand and Stuart Robinson in the early 1970s. The goal of this design was to create a fast, inexpensive airplane that was easy to build. The simple construction of spruce wood and fiberglass made this kit an ideal project for first-time builders. A 65 HP Volkswagen engine provided enough thrust to reach a maximum straight and level speed of 200 MPH with two passengers, as published. Since its inception, many builders have modified the design to accommodate larger engines. My father purchased his KR-2 kit with construction in progress from Hal Boyle. Hal had decided to build this aircraft with a larger engine as well, mainly for the purpose of providing better performance at higher altitudes as would be required to fly to the airport at 6260 feet elevation in South Lake Tahoe, a favorite weekend destination.

In this case, an 85 HP Continental engine has been purchased for use on the aircraft. The added weight and thrust of a more powerful engine requires a greater load-carrying construction and more lift from the wings. To allow more room for the passengers, the canopy is heightened two inches and the fuselage is made 6.5 inches wider. These changes to the design have been made on recommendations from other builders, whose altered KR-2s have flight characteristics largely based on trial and error.

An aerodynamic analysis has been performed on a modified kit plane design. Various software tools, as well as empirical and analytical means of analysis have been utilized. The focus of the study is a modified KR-2 homebuilt kit plane in construction. A

literature review presents the performances published by other builders for similar airplanes and also presents research findings from an accident report investigation for similar airplanes. Analysis of the design begins with a weight and balance calculation, followed by an estimation of the static margin. A study of the airfoil is performed with comparison to an alternate airfoil that was designed for the KR. Wing lift distribution for the specific non-uniform taper and twist of this wing is found via a computational fluid dynamic (CFD) study using the *Fluent* software suite with *Gambit* mesher. This result is compared to the lift distribution from a derivation obtained from combining potential flow theory with trailing vortices theory, and this calculation is outlined in detail. The Roskam Class II drag polar estimation is obtained for a range of speeds at altitude of 6000 feet. Several performance parameters are calculated.

II. List of Symbols

a = lift curve slope

b = wingspan

bhp = engine shaft brake horsepower

c = chord length

$\bar{c}$ = mean geometric chord

C_f = turbulent flat plate friction coefficient

C_L = coefficient of lift

C_D = coefficient of drag

CG = center of gravity

D = drag

d_f = maximum fuselage diameter

EW = empty weight

h = CG location, fraction of $\bar{c}$

h_{ac} = aerodynamic center location, fraction of $\bar{c}$

h_n = neutral point location, fraction of $\bar{c}$

L = lift

LE = leading edge

m = lift curve slope

OEW = operating empty weight

P = air pressure

P_A = power available

P_R = power required

$\bar{q}$ = dynamic viscosity

R = leading edge suction parameter

R_{wf} = wing - fuselage interference factor

Re = Reynolds number

R/C = rate of climb

s = 1/2 wingspan

s_{LO} = lift off distance

S = wing area

$\mathrm{S_{wet}}$ = wetted area

t/c = thickness ratio

T = thrust

TVT = trailing vortices theory

TOW = take off weight

V_∞ = free stream velocity

α = geometric angle of attack

α_0 = effective angle of attack

$\alpha_{C_L=0}$ = zero lift angle of attack

ε = span efficiency factor

ε_t = wing twist angle

η = propeller efficiency

η = drag of finite cylinder / drag of infinite cylinder

κ = vortex strength

κ_0 = local vortex strength

λ = taper ratio

Λ = sweep angle

μ = dynamic viscosity for air

υ = induced drag factor due to linear twist

ρ_∞ = air density

III. Introduction

A. Personal Background

Aviation has been in my family since I can remember. My father was an avid pilot when I was very young, and we took many adventures as a family in Cessna 172s. At first my time was spent building custom paper airplanes, and from there I graduated to remote control airplanes.

My entire education has been local to San Jose, CA. I attended Northwood Elementary School, then Morrill Middle School, where I was Salutatorian, and received the Outstanding Musician award for my participation as a violinist in the orchestra. At Independence High School I was drawn toward math and physics.

San Jose State University interested me because it was the only local university with an aviation program. I complemented my aviation studies with participation in the SJSU Symphony for several semesters. I received my Bachelor of Science degree from San Jose State University in Aviation Operations, Maintenance Management option in December of 1999. In addition, I obtained an Airframe Mechanic certification. My Airframe certification allowed me to work as an aircraft mechanic at Inbound Aviation of Reid Hillview Airport, where we maintained a small fleet of small aircraft available for rent. The Aviation program at SJSU was challenging, and provided me with a good foundation in a technical *applied* science.

However, I wanted to further my education with an engineering degree, and began taking prerequisites for a Master's Degree in Mechanical Engineering. My focus in graduate work has been in fluids and heat transfer, with electives in aerospace engineering coursework including aircraft structures and aerodynamics.

B. Motivation for this Project

The motivation for doing this project comes from a desire to further my knowledge of aerodynamics. I am also fueled by the need to make intelligent choices for the construction of this aircraft.

C. First Semester Master's Project with Boris Bravo

Much of the credit for the work on this project goes to Boris Bravo, who worked with me during the first semester (course ME295B). During the first semester, we

developed preliminary airfoil characteristics, wing lift distribution with the Trailing Vortices Theory, and the aircraft drag polar. His expertise on the subject of aerodynamics has been invaluable in this learning experience.

D. Goal of Project

My approach, as an engineer, is to analyze the design in its current state, and to make appropriate recommendations to verify the airworthiness of this particular modified KR-2 aircraft.

E. Hal and Jan

In the early 1980s in San Jose, California, Hal Boyle began the construction of his second homebuilt aircraft. As an excellent craftsman, he diligently crafted a fuselage with incredible symmetric precision and attention to detail. My father, Jan Nordin, was at the time an avid pilot flying mainly out of Reid Hillview Airport in East San Jose. Jan is also a great craftsman, and at that same time developed interest in homebuilt, experimental aircraft. He joined a local club for homebuilt aircraft enthusiasts, EAA (Experimental Aircraft Association) Chapter 338. There he met Hal at a monthly meeting. Jan offered to help with the construction of this aircraft, and together they completed the front and rear spars, the cowling, the beginnings of a propeller, and installed tail group control cabling to the fuselage.

F. The KR-2

The homebuilt aircraft under construction in Hal's garage was a modified version of the KR-2, a two seat (side by side) high speed low-wing monoplane. Jan was particularly interested in this design because the KR-2 is designed for the first time builder, having a simple, elegant assembly of wood, foam, and fiberglass. Ken Rand of Rand-Robinson Engineering designed the original single seat KR series aircraft in 1972. The KR design was a breakthrough in homebuilt kit technology when it became available to the homebuilt builder, pioneering the use of "state-of-the-art foam-and-fiberglass composite construction method which has now become standard in homebuilt, commercial, and military aircraft. Its strength-to-weight ratio is superior to conventional construction methods."[1]

[1] KR Home Page http://www.fly-kr.com

The KR series has three high speed aircraft capable of 200 mph. The KR-1 seats only the pilot. The KR-2 was later designed for two passengers. The KR-2S ('S' for stretched) was offered much later as a two-seater with added leg and head room for the passengers in response the high number of builders modifying the KR-2 for added comfort. Specifications for the KR series kit planes are shown in Table 1. Note that the published performances of all three models are very similar, with cruise speed of 180 mph, take off distance of 350 ft., and 52 mph stall speed.

The high popularity of the KR-2 in the 1980's was due to several factors, including the ease of construction, low cost, high speed, and the ease of ability to customize the design. High speed can be seen by comparing the cruise speed of the KR-2 to that of a Cessna. The KR-2 has a published cruise speed of 180 mph with a 65 HP VW 2100 engine. In comparison, the popular Cessna 172 cruises at only 150 mph with a 195 HP Continental IO-360 engine. Part of the scope of this project is to estimate the cruise speed for the modified KR-2.

KR Series Aircraft Specifications			
	KR-1	KR2	KR2-S
Length	12' 9"	14' 6"	16'
Wing Span	17' 0"	20' 8"	23'
Total Wing Area	62 sq. ft.	80 sq. ft.	82 sq. ft.
Empty weight	375 lbs.	480 lbs.	---
Gross weight	750 lbs.	900 lbs.	980 lbs.
Useful load	375 lbs.	420 lbs.	460 lbs.
Baggage capacity	20 lbs. max	35 lbs. max	35 lbs.
Take off distance	350 ft.	350 ft.	350 ft.
Landing distance	900 ft.	900 ft.	600 ft.
Stall Speed	52 mph	52 mph	52 mph
Maximum Speed	200 mph	200 mph	200 mph
Cruise Speed	180 mph	180 mph	180 mph
Range	1400 miles	1600 miles (35 gal. fuel)	1080 miles
Rate of Climb (light)	1200 fpm	1200 fpm	1200 fpm
Rate of Climb (gross)	800 fpm	800 fpm	800 fpm
Service ceiling	15,000 ft.	15,000 ft.	15,000 ft.
Engine	VW 1834	VW 2100	VW 2180, Subaru EA-81, Continental O-200
Fuel	8-30 gal.	12-35 gal.	---
Fuel consumption	3.8 gph	3.8 gph	3.8-5.5 gph (depending on engine)
Seating	1	2 across	2 across
Landing Gear	Fixed conventional or trigear, or retractable conventional	Fixed conventional or trigear, or retractable conventional	Fixed conventional

Table 1: KR Series Aircraft Specifications[2]

[2] Specifications taken from http://www.fly-kr.com KR1,KR2, KR2-S links

G. *Design Changes*

Hal was, as many other builders, not pleased with the tight quarters in the cockpit, and expanded the fuselage layout to allow for more elbow room and head room. (At the time, the roomier KR-2S was not yet available. The KR-2S was noted in a 1993 *Sport Aviation* article as being 'new'.[3]) 6.5 inches were added to the width of the fuselage and the canopy was raised by 2 inches. This is a substantial increase in maximum cross-sectional area. To account for the increase in fuselage drag, he decided to increase the horsepower of his KR-2 by 25% by upgrading the VW 2100 to a Continental C-85. These modifications were made by Hal in the early stages of the project. In addition to the upgraded engine and expanded fuselage, Hal and Jan made other modifications to assure that the structural integrity of the aircraft would be intact with the larger loads that come with the larger engine and expanded fuselage. The truss sections were strengthened at every joint as shown in Figure 2 with extra spruce plywood reinforcements. All wood members were glued together under a clamping force with an aircraft specific slow-cure two-part epoxy.

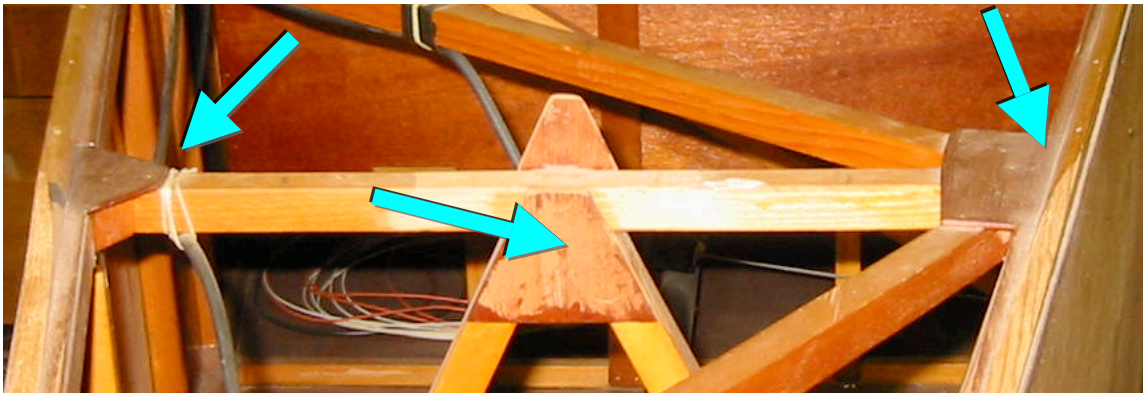

Figure 2: Reinforced Truss Joints

The wing spars were lengthened and hence the wing area was increased. This was done to maintain a similar wing loading to the original design. As shown in

Equation 1, the wing loading has been increased, increasing the stress on wing structure. Note that all dimensional values for the modified KR-2 are derived in Chapter V, Configuration. Gross weight is estimated in Chapter VI, Weight and Balance.

[3] "KR-2S," *Sport Aviation*, July 1993, p. 38.

$$\text{Wing Loading} = \frac{\text{Gross Weight}}{\text{Wing Area}}$$

$$\text{Wing Loading}_{KR2} = \frac{900 \text{ lb}}{80 \text{ ft}^2} = 11.25 \text{ psi} \qquad \textbf{Equation 1}$$

$$\text{Wing Loading}_{KR2\ MOD} = \frac{950 \text{ lb}}{86.4 \text{ ft}^2} = 12.42 \text{ psi}$$

Figure 3 shows the construction project in its current state, with 95% of the wood construction complete, canopy section formed, and tail section ready to glass. Note the flanges where the outer wing spars attach. Also note the main landing gear. Leveraging the experience gained while helping other builders with KR projects that had the tendency to tip over tendency on the ground, Hal and Jan upgraded the landing gear with larger struts and wheels, borrowed from the Minicab design. The main wheels are moved forward to reduce the tip over tendency. The KR-2 also has removable outer wing sections. Note the mounting flanges. Figure 4 shows the upgraded engine, ready for final inspection. Additional photos of the construction are posted in the Appendix.

Figure 3: Fuselage Boat Section with Canopy, Main Struts, and Landing Gear

Figure 4: Continental C-85 Engine, Rebuilt with Zero Hours

H. A Look at the KR2-S

The KR series aircraft are famous for their pitch sensitivity. A look at the KR-2 characteristics listed in Table 1 shows that the KR-2S has many of the similar modifications that this modified KR-2 has: with more room for the passengers, a greater wingspan, and a larger engine. The exception is that the overall fuselage length has been stretched by 18 inches. Therefore, the KR-2S is likely much more stable than our modified KR-2 design with less pitch sensitivity.

IV. Literature Review

A. Other KR-2 Builders' Modifications and Performance

The KR-2, as previously stated, is a popular homebuilt airplane kit. It is important to consider the published modifications and performance achieved by other builders. I have researched articles from *Sport Aviation*, a monthly EAA membership magazine, to collect data about other KR-2s. The performances of these other airplanes are used in this project for validation of the analysis of our modified KR-2.

Seven designs have been reviewed, and there are interesting trends to note. Reference the tabulation of modifications and performance data from these aircraft in Table 5, Appendix B. With hundreds of homebuilt sport plane kits available, the KR design was chosen due to the ease of construction, low cost, and high speed. Almost every article noted that pitch sensitivity was an issue. Two of the builders (pre KR-2S availability) extended the fuselage to decrease the pitch sensitivity. One was stretched by 13.5 inches, and the other was stretched by 21 inches to add longitudinal stability.

Maximum speed of the aircraft researched range from 155 to 197 mph. The aircraft with 80 HP engines average 173 mph maximum speed. This contradicts early predictions that the cruise speed with the upgraded engine would have a higher maximum speed than the specified 200 mph. Instead, these aircraft have a lower maximum speed. With specified cruise speed of 180 mph, a faster 190 mph cruise was predicted with our C-85 engine. This may be due to the extra weight of additional modifications.

B. NTSB Crash Report Summary

In addition to looking at other KR-2 aircraft that have performance numbers and modifications published, an investigation of crash reports has been made with data supplied by the National Transportation Safety Board's Aviation Accident Database Query. "The NTSB aviation accident database contains information from 1962 and later about civil aviation accidents and selected incidents within the United States, its territories and possessions, and in international waters."[4]

It was extremely surprising to see how many accidents have been documented with the KR-2. In the seven year period from the release of the KR-2, there were 50 accidents with fatalities in 15 of the 50 accidents. This is a fatality rate of 30%. The time span for the data is from 1977 to 1984. To compare this figure with the data from a non-experimental aircraft, the Cessna 152 had 1016 accidents for the same time period with fatalities in 107 of the accidents. This, in comparison, is only a fatality rate of 10.5%, one third the rate of the KR-2! It is well known that experimental aircraft have much higher accident rates than general aviation aircraft, and this investigation reveals causes unique to experimental aircraft.

The cause of the accidents for the KR-2 has been grouped by pilot error, construction (builder error), engine failure, and maintenance error. Figure 5 is a comparison of the number of accidents by each cause group. Note that pilot error is the largest cause group and accounts for 26 out of 50 accidents. Construction or builder error is the second largest cause group, and accounts for 8 accidents. Of the pilot errors, many of these are due to lack of familiarity with the aircraft and failing to maintain control of the aircraft, alluding to the need for taking exceptional precautions with experimental aircraft.

[4] NTSB - Aviation Accident Database Query. http://www.ntsb.gov/ntsb/query.asp. 11-26-06

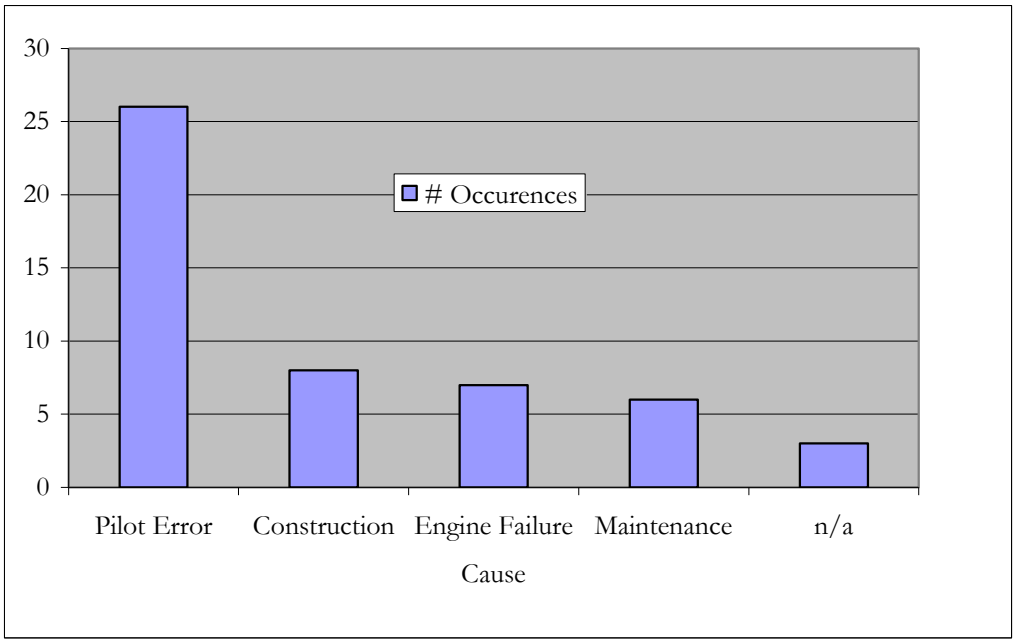

Figure 5: KR-2 Accidents from 1977-1984 Grouped by Root Cause[5]

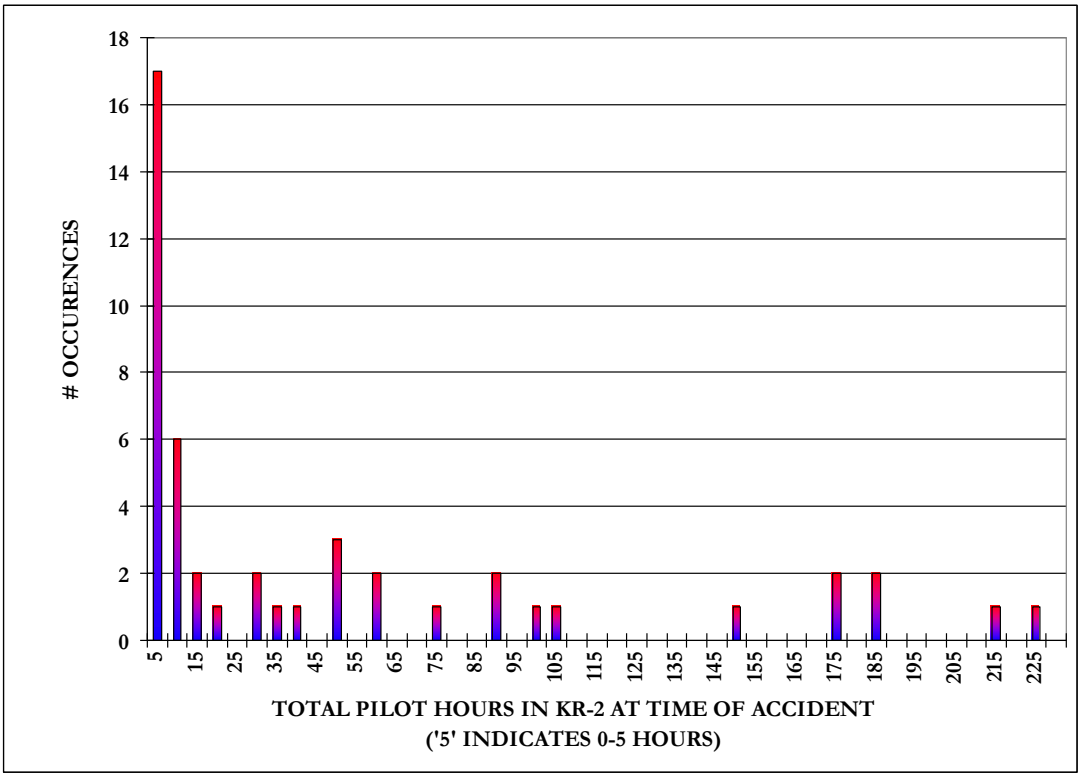

Figure 6: Histogram - # Occurrences for Total Pilot Hours in KR-2 at Time of Accident

[5] NTSB - Aviation Accident Database Query. http://www.ntsb.gov/ntsb/query.asp. 11-26-06

As seen from the reports, even very seasoned pilots crashed a KR-2 within the first hours of attempting to fly a KR-2. For example, a pilot with 1,300 hours of total flight time crashed a KR-2 within the first hour on January 20, 1979.[6] Unfortunately in this case, the pilot was killed. The root cause was pilot error - stalling during a maneuver.

Figure 6 shows a histogram of the number of occurrences of accidents binned by total flight hours the pilot had in a KR-2 at the time of the accident. An amazing fact revealed from this figure is that the accident rate is extremely high during the first few flights. 17 of the 50 accidents (35%) occurred during the first 5 hours of flight time in a KR-2. A more detailed description of each crash investigated follows in Figure 7.

[6] NTSB - Aviation Accident Database Query. http://www.ntsb.gov/ntsb/query.asp. 11-26-06

Accident #	Date	# Deaths	Flight Purpose	Cause	Detail	A/C Data	Pilot Hrs Total	Pilot Hrs in Make/Model
1	9/23/1976	0	Pleasure	Pilot Error	Premature Lift Off	Substantial	99	30
2	3/29/1977	1	Test	Pilot Error	Not Familiar w/ AC	Destroyed	1524	9
3	7/17/1977	0	Pleasure	Pilot Error	Misjudged distance/altitude	Substantial	600	6
4	7/24/1977	1	Instruction	Pilot Error	Poor Planning	Destroyed	3000	1
5	5/11/1978	0	Instruction	Maintenance	Poor Maintenance	Destroyed	12300	90
6	5/30/1978	0	Pleasure	Pilot Error	Fly with known problems	Substantial	185	57
7	9/14/1978	0	Test	Construction	Poor Construction	Substantial	52	0
8	10/9/1978	0	Pleasure	Maintenance	Poor Maintenance	Destroyed	78	0
9	12/7/1978	0	Test	Construction	Poor Construction	Substantial	500	6
10	1/20/1979	1	Pleasure	Pilot Error	Stall during maneuver	Destroyed	1300	1
11	1/31/1979	1	Pleasure	Engine Failure	Unknown	Destroyed	975	174
12	5/12/1979	0	Pleasure	Engine Failure	Material Failure	Destroyed	2500	50
13	6/10/1979	0	Practice	Pilot Error	Land w/ gear up	Substantial	1287	1
14	8/14/1979	0	Pleasure	Construction	Material Failure	Substantial	275	97
15	8/22/1979	2	Test	Pilot Error	Weight and Balance	Destroyed	144	0
16	10/10/1979	0	Test	Pilot Error	Fail to abort take-off	Destroyed	80	11
17	11/11/1979	2	Pleasure	Pilot Error	Spin/stall	Destroyed	700	n/a
18	1/29/1980	0	Pleasure	Construction	Poor Construction	Destroyed	300	103
19	3/14/1980	0	Test	Construction	Aileron Imbalance	Destroyed	2354	2
20	5/14/1980	0	Test	Construction	Fuel starvation	Substantial	140	0
21	6/17/1980	0	Pleasure	Construction	Wrong engine part	Substantial	570	26
22	7/6/1980	2	Pleasure	Pilot Error	Fuel starvation	Destroyed	329	3
23	10/12/1980	0	Pleasure	n/a	n/a	Substantial	1287	3
24	5/28/1981	0	Pleasure	Pilot Error	Collision w/ aircraft	Destroyed	165	47
25	7/12/1981	1	Test	Engine Failure	n/a	Destroyed	n/a	n/a
26	7/20/1981	0	Pleasure	Pilot Error	Fly with known problems	Substantial	460	172
27	8/2/1981	0	Test	Pilot Error	Fly with known problems	Destroyed	130	1
28	8/16/1981	1	Test	Pilot Error	Spin/stall	Destroyed	133	0
29	8/30/1981	0	Pleasure	Pilot Error	Failed to see obstacle	Substantial	147	75
30	9/10/1981	0	Test	Pilot Error	Fly with known problems	Destroyed	5960	0
31	11/15/1981	0	Pleasure	Pilot Error	Vortex turbulence	Substantial	104	10
32	12/20/1981	0	Pleasure	Maintenance	Poor Maintenance	Substantial	126	13
33	4/24/1982	0	Pleasure	Pilot Error	Fail to maintain airspeed	Substantial	66	10
34	6/5/1982	0	Pleasure	Pilot Error	Proper altitude not maintained	Substantial	1033	212
35	6/6/1982	2	---	Pilot Error	Fuel starvation	Destroyed	160	89
36	6/11/1982	0	---	Pilot Error	Spin/stall	Substantial	234	48
37	7/1/1983	0	---	Construction	Uncertified component failure	Destroyed	1760	57
38	10/6/1982	0	---	Pilot Error	Fuel starvation	Destroyed	416	16
39	12/12/1982	2	---	Pilot Error	Spin/stall	Destroyed	314	185
40	12/18/1982	0	---	Engine Failure	n/a	Destroyed	260	146
41	6/1/1983	0	---	Engine Failure	Poor Maintenance	Substantial	300	4
42	7/19/1983	0	---	Pilot Error	Fail to maintain airspeed	Substantial	775	35
43	7/21/1983	0	---	Maintenance	Poor Maintenance	Substantial	120	3
44	9/4/1983	0	---	Maintenance	Poor Maintenance	Substantial	6443	38
45	11/6/1983	1	---	n/a	n/a	Destroyed	225	225
46	1/21/1984	2	---	Pilot Error	Failed to see obstacle	Destroyed	n/a	n/a
47	2/26/1984	1	---	Maintenance	Improper mixture	Destroyed	221	5
48	3/20/1984	0	---	Engine Failure	n/a	Destroyed	864	2
49	7/29/1984	0	---	Engine Failure	Oil leak	Substantial	2138	182
50	8/12/1984	0	---	n/a	n/a	Destroyed	78	10

Figure 7: Summary of 50 Consecutive KR-2 Accident Reports from 1977 to 1984[7]

[7] NTSB - Aviation Accident Database Query. http://www.ntsb.gov/ntsb/query.asp. 11-26-06

V. Configuration

The modified KR-2 has a basic low wing, fixed conventional gear configuration. Figure 8 shows the component layout for the engine group, front fuel tank, instrument panel, seating, baggage, battery, and the location of the firewall. The firewall will serve as the datum for the weight and balance calculation.

The engine group is comprised of the Continental C-85, a starter motor, two magnetos, and the engine mount. The front fuel tank is in front of the instrument panel, and has a capacity of 14.6 gallons. The instrument panel consists of only the basic requirements for VFR flight. Seating is side by side with the control stick in the center of the seat and throttle on both sides of the cockpit. The baggage compartment is directly behind the seat, and the battery is located in the rear section of the fuselage.

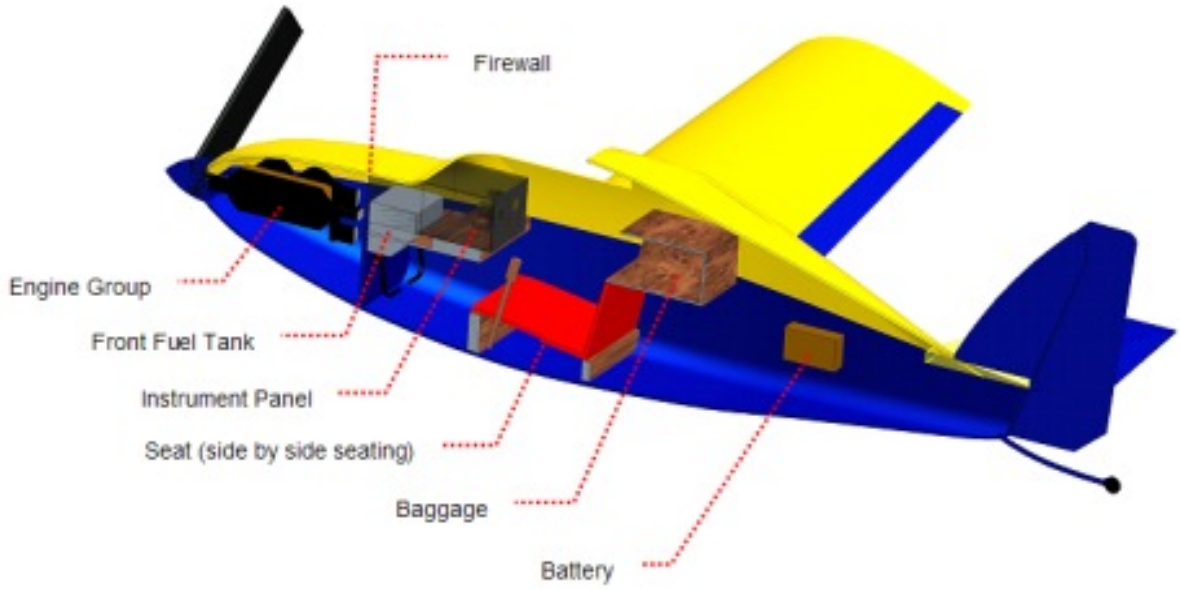

Figure 8: Cutaway View of Modified KR-2 Showing Component Placement

The following two figures show the placement of the wing fuel tanks, which are located between the forward and aft wing spars in the inboard straight section of the wings. Their combined capacity is 14.1 gallons of fuel.

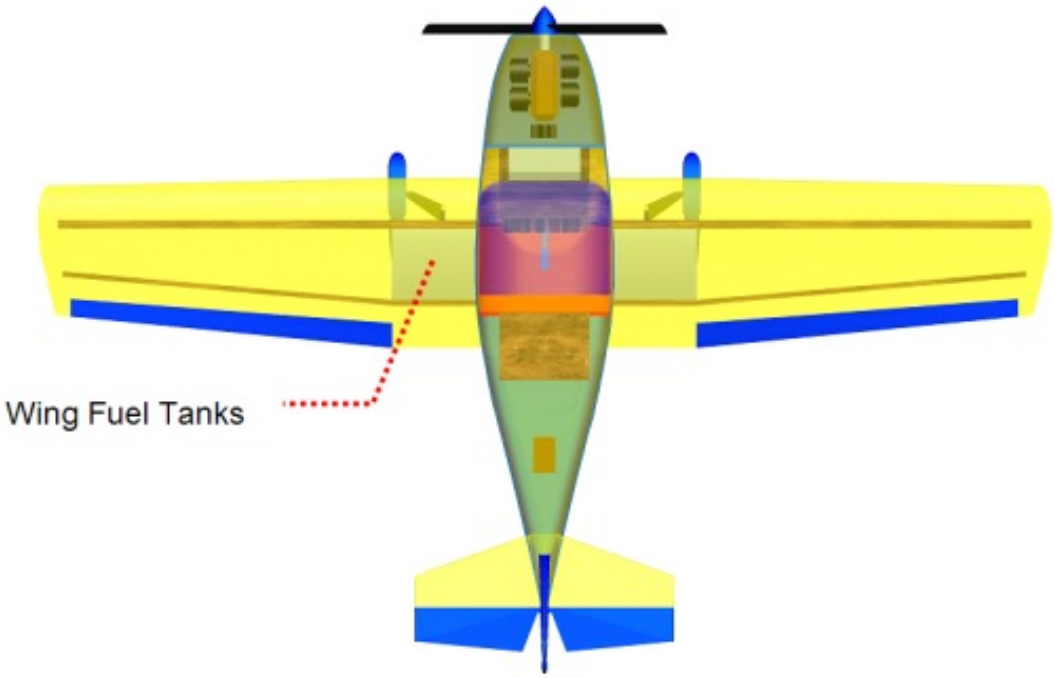

Figure 9: Top View, Transparent

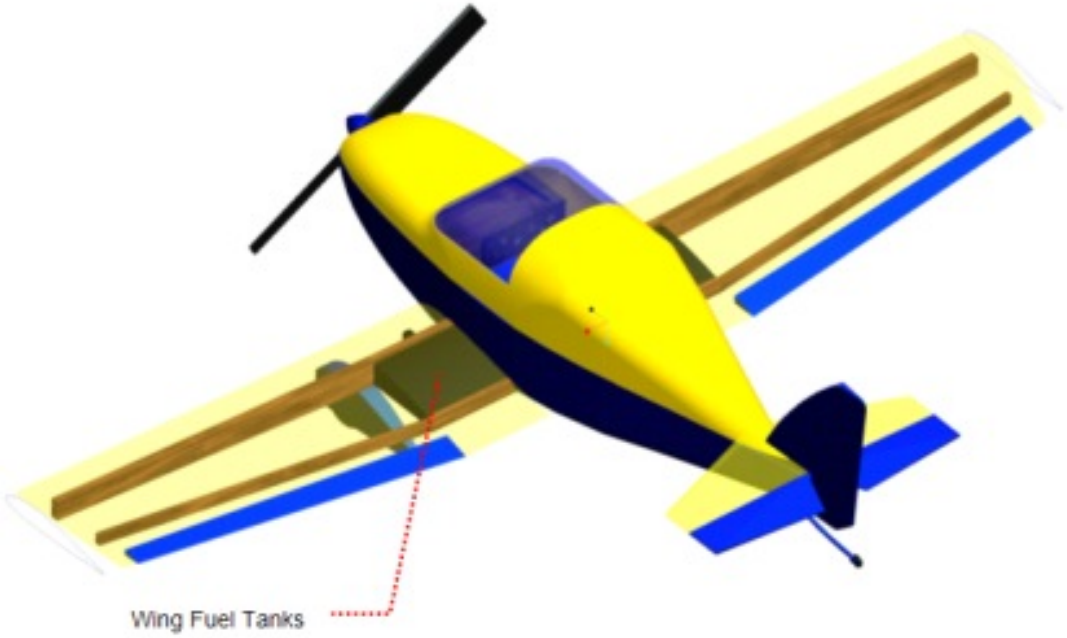

Figure 10: Top Isometric View with Transparent Wings

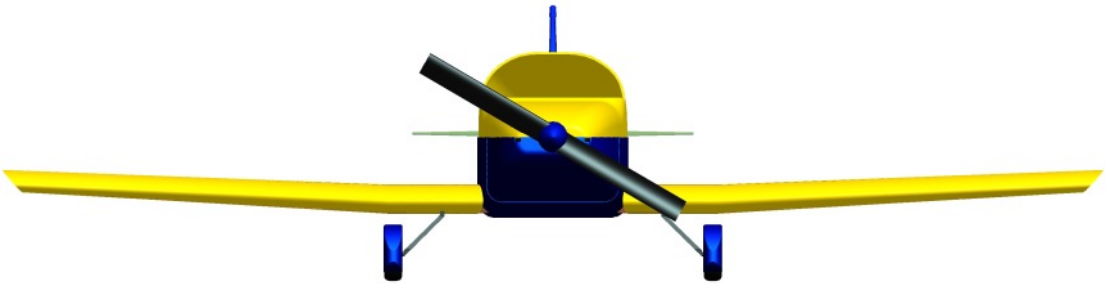

Figure 11: Front View

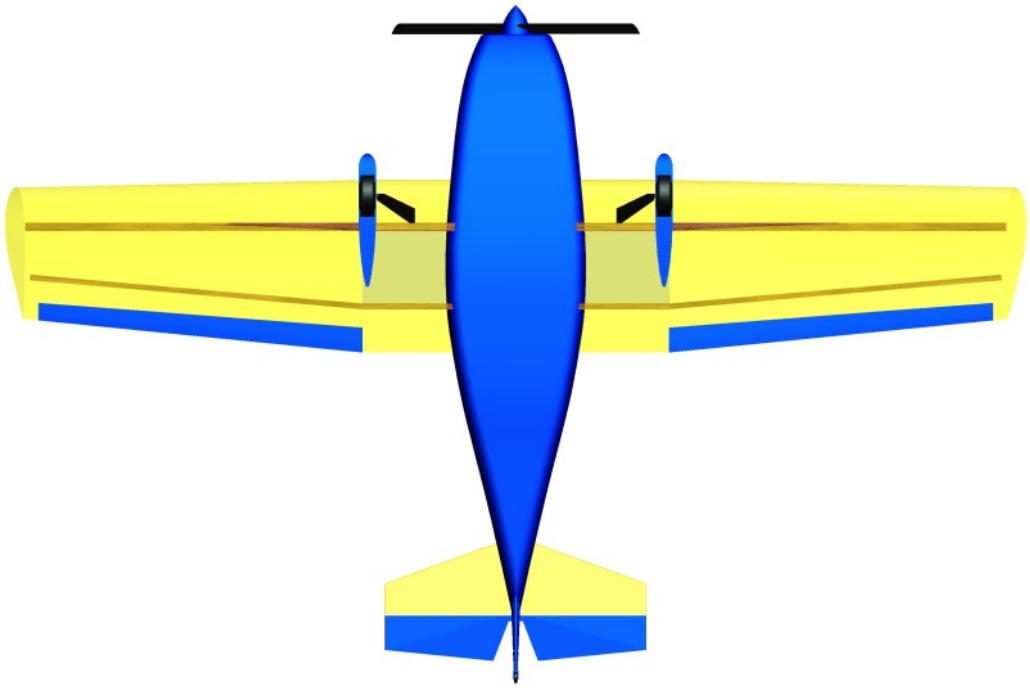

Figure 12: Bottom View Showing Wing Spars (note: front spar at ¼ chord; ¼ chord sweep angle = 0)

Dimensioned drawings of the aircraft follow in inches. From the layout, basic configuration parameters for the wing and the empennage are determined. Drawings were created with *Pro-Engineer*.

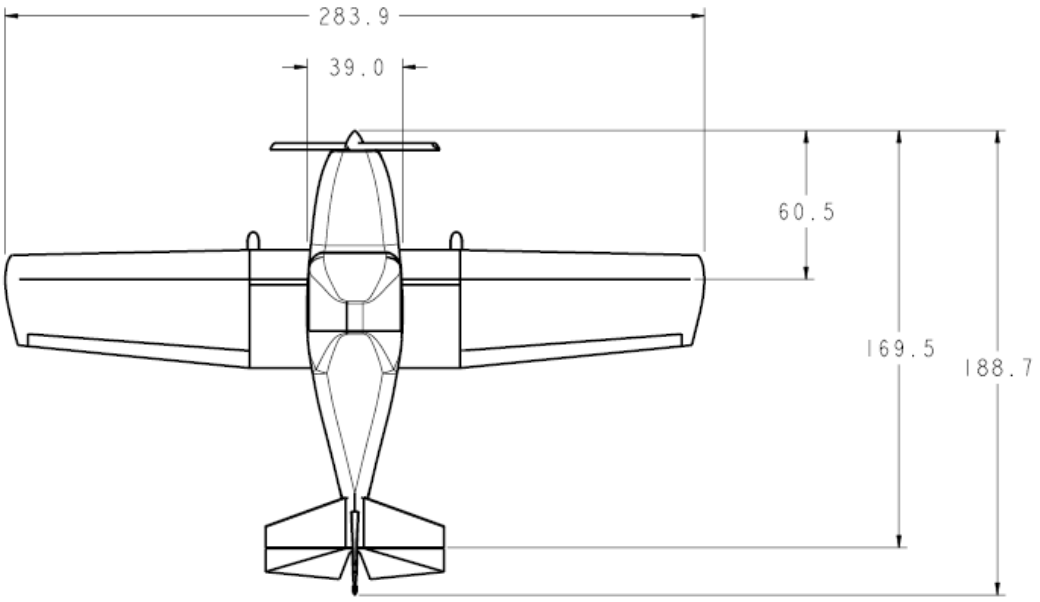

Figure 13: General Dimensions – Top View

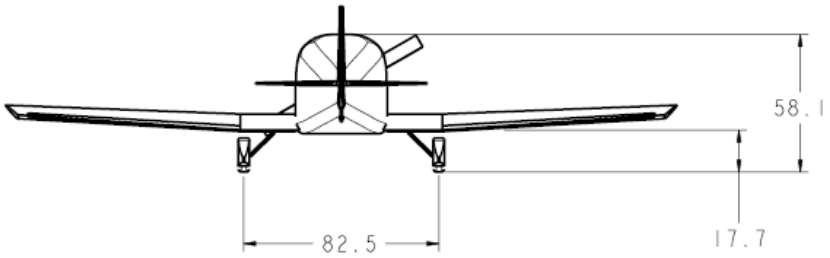

Figure 14: General Dimensions, Back View

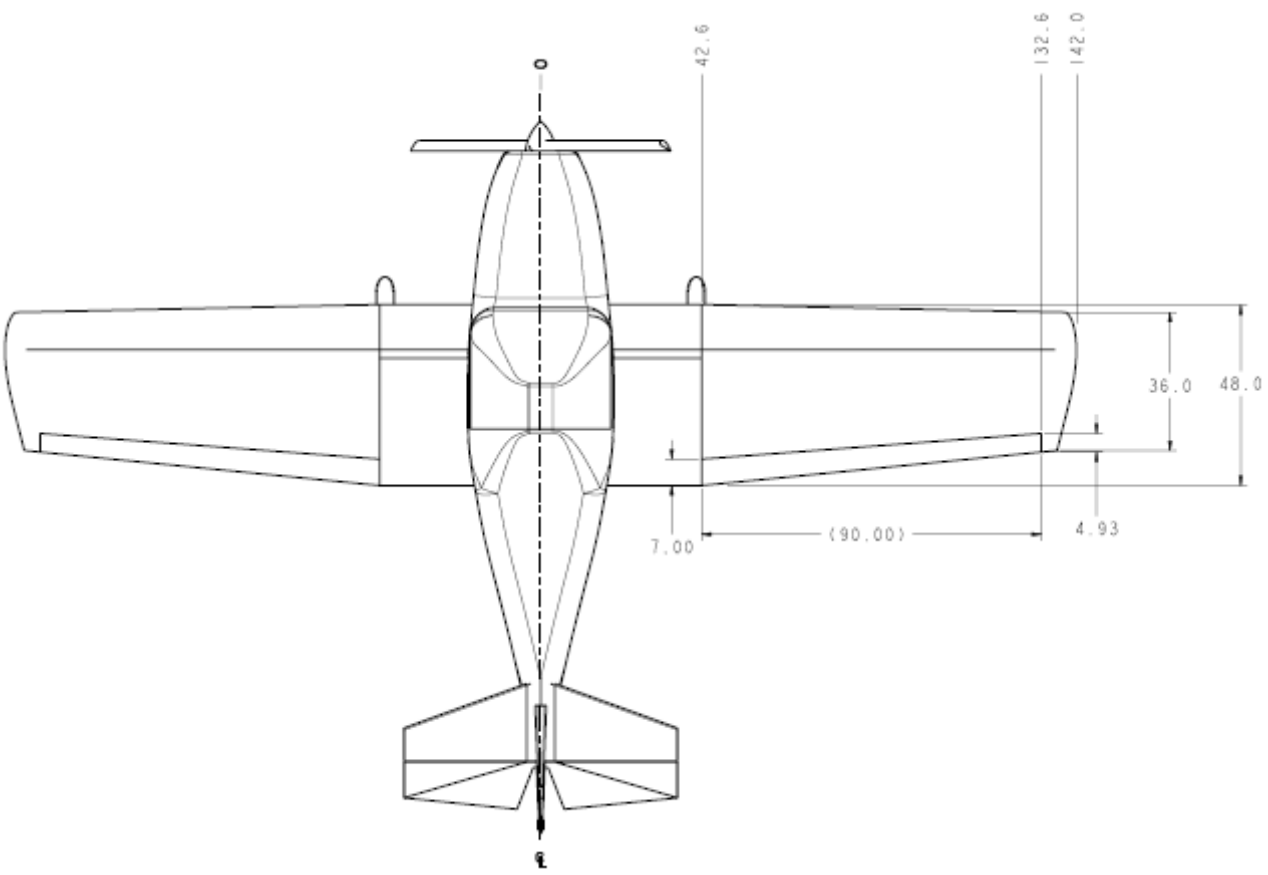

Figure 15: Wing Planform Dimensions

The wing parameters are calculated as a function of geometry. Since the wing has non-uniform taper and twist, some parameters need to be calculated for the equivalent straight, tapered wing as shown in Figure 16.

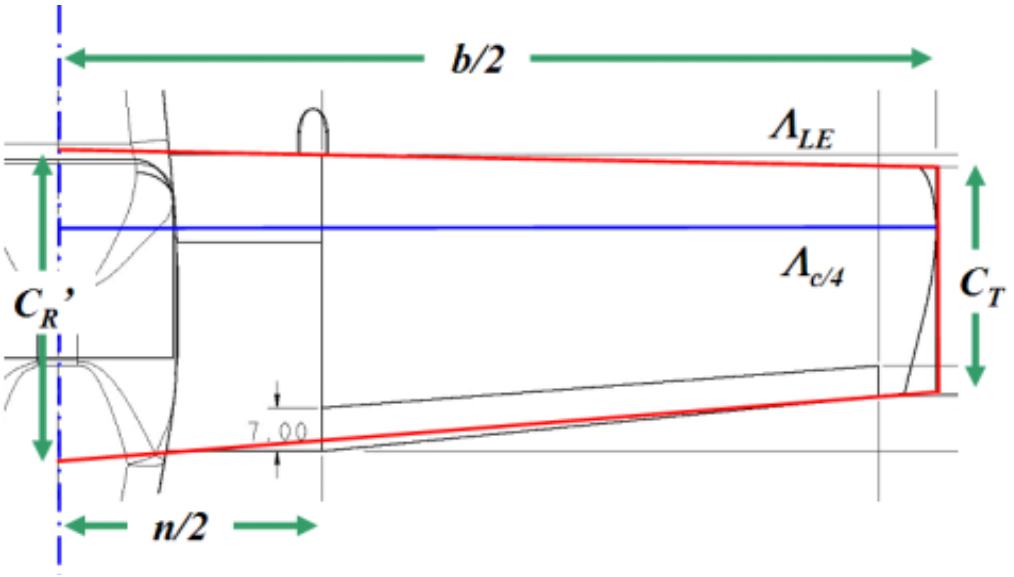

Figure 16: Equivalent Wing Planform (Half-Symmetric)

- Wingspan $b = 284 \text{ in} = 7.21 \text{ m}$
- Geometric Chord at root $C_R = 48 \text{ in} = 1.22 \text{ m}$
- Geometric Chord at tip $C_T = 36 \text{ in} = 0.91 \text{ m}$
- Wing Area $S = 12440 \text{ in}^2 = 8.03 \text{ m}^2$
- Wetted Wing Area[8]

$$S_{wet_W} = 2S\left\{1 + 0.25(t/c)_r \frac{1 + (t/c)_{tip}/(t/c)_{root}\,\lambda}{1+\lambda}\right\}$$

$$S_{wet_W} = 2(8.03 \text{ m}^2)\left\{1 + 0.25(.150)\right\}$$

$$S_{wet_W} = 16.66 \text{ m}^2$$

- Aspect Ratio $A = b^2 / S = 6.47$
- Equivalent Wing Planform:

  The equivalent wing planform assumes a shape based on equivalent areas per Figure 16. $n/2 = 1.082 \text{ m}$ and indicates location where the change in shape of the wing occurs. Assuming the tip chord and wingspan remain constant, the equivalent root chord, C_R, is calculated:

$$S_{original} = C_T b + n(C_R - C_T) + (b-n)(C_R - C_T)/2$$

$$S_{equivalent} = C_T b + (C_R' - C_T) b/2$$

  Solving for C_R':

$$C_R' = 1.31 \text{ m}$$

- Taper Ratio $\lambda = C_T / C_R' = 0.698$
- ¼ Chord Sweep Angle $\Lambda_{c/4} = 0$
- Leading Edge Sweep Angle $\Lambda_{LE} = 1.57^\circ$ from equivalent geometry
- Wing Twist Angle $\varepsilon_T = -3.0^\circ$ (washout)

[8] Roskam, Jan. Airplane Design, Part VI. Appendix B. Lawrence, 1990.

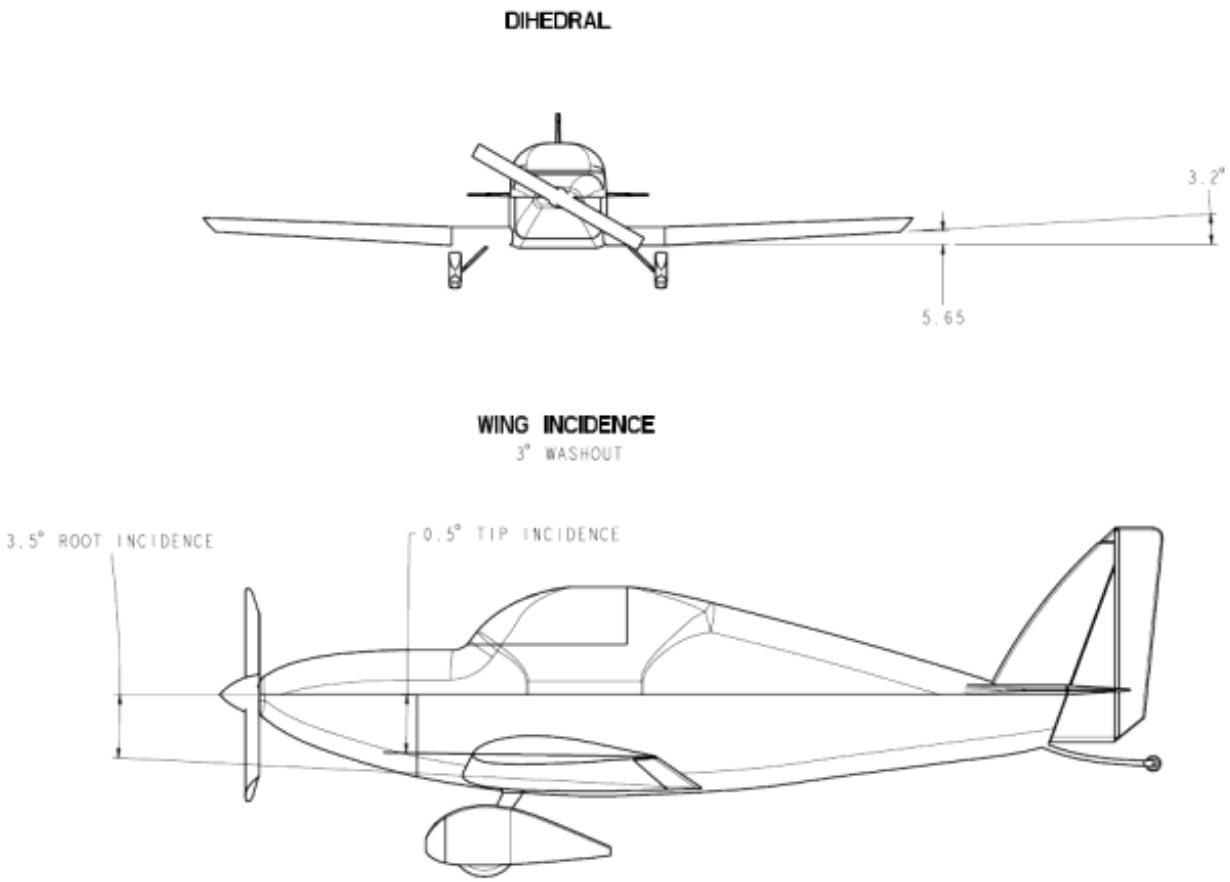

Figure 17: Dihedral and Wing Incidence

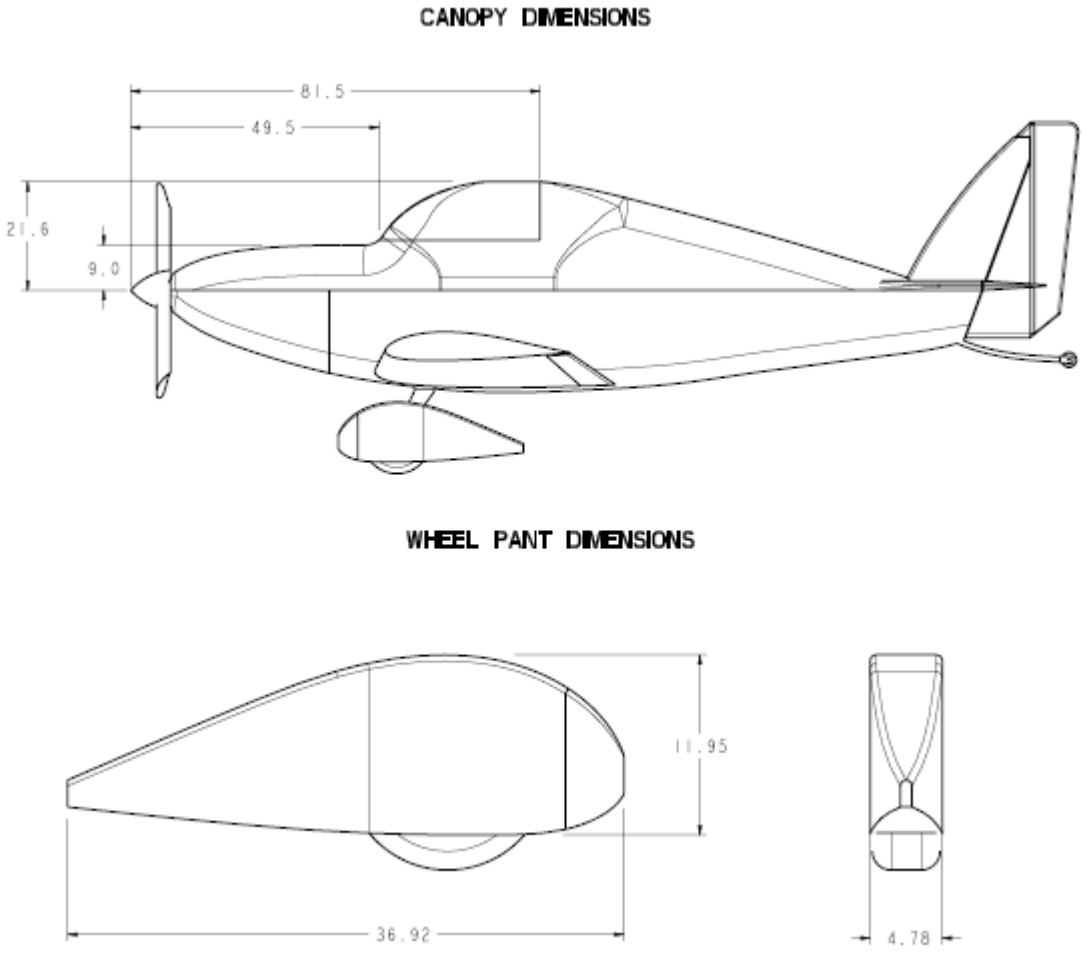

Figure 18: Canopy and Wheel Pants Dimensions

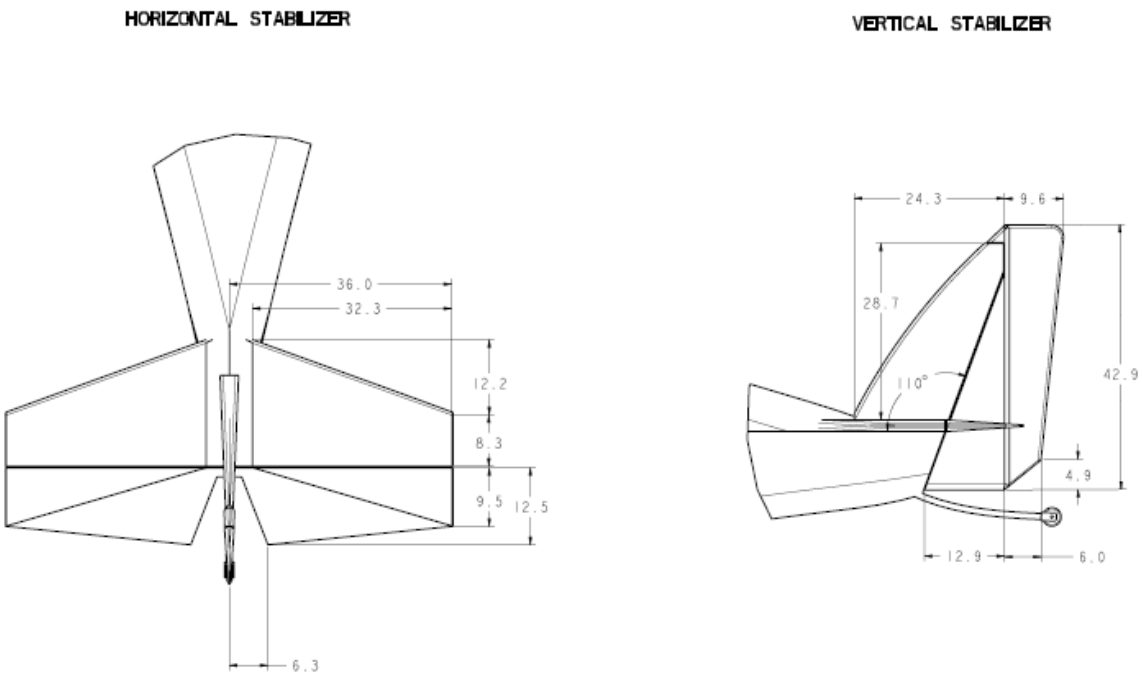

Figure 19: Empennage Dimensions

The empennage parameters are presented here for later use in the lift and drag calculations.

- Horizontal Stabilizer Area $S_h = 1760 \text{ in}^2 = 1.135 \text{ m}^2$
- Horizontal Stabilizer Wetted Area $S_{h_{WET}} = 2.1 \times S_h = 3696 \text{ in}^2 = 2.384 \text{ m}^2$
- Horizontal Stabilizer Thickness Ratio $(t/c)_h = 0.065$
- Horizontal Stabilizer Incidence Angle $i_h = 0^o$
- Horizontal Stabilizer Mean Geometric Chord $\bar{c}_h = 0.689 \text{ m}$
- Vertical Stabilizer Area $S_v = 880 \text{ in}^2 = 0.568 \text{ m}^2$
- Vertical Stabilizer Wetted Area

  $S_{v_{WET}} = 2.1 \times S_v = 1848 \text{ in}^2 = 1.192 \text{ m}^2$
- Vertical Stabilizer Thickness Ratio $(t/c)_v = 0.070$
- Vertical Stabilizer Mean Geometric Chord $\bar{c}_v = 0.635 \text{ m}$

VI. Weight and Balance

A weight and balance analysis is performed in order to determine if the locations chosen for the components will yield a stable aircraft. Starting with the base empty weight of the unmodified KR-2 at 480 lb, a rough estimate of the new empty weight accounts for the change in engine weight and adds 10% for the larger fuselage and wing structure.

$$EW_{MOD} = EW_{KR2} - W_{VW} + W_{C85} + .1(EW_{KR2})$$
$$EW_{MOD} = 480 - 163 + 204 + .1(480)$$
$$EW_{MOD} = 569 \text{ lb}$$

The following detailed weight and balance analysis will show an empty weight of 551 lb, close to this estimate.

Figure 21 illustrates the locations of major components on the aircraft per current construction plans. The fuselage in its current state of construction was weighed on a bathroom scale to get the weight on the main wheels and on the tail wheel. The tail of the wheel was lifted so that the fuselage was level with the ground. The main wheels each had a 71 lb load, and the tail wheel carried a 28 lb load, for a total 'construction-in-progress' fuselage weight of 170 lb.

Figure 20: Right Main Wheel on Scale

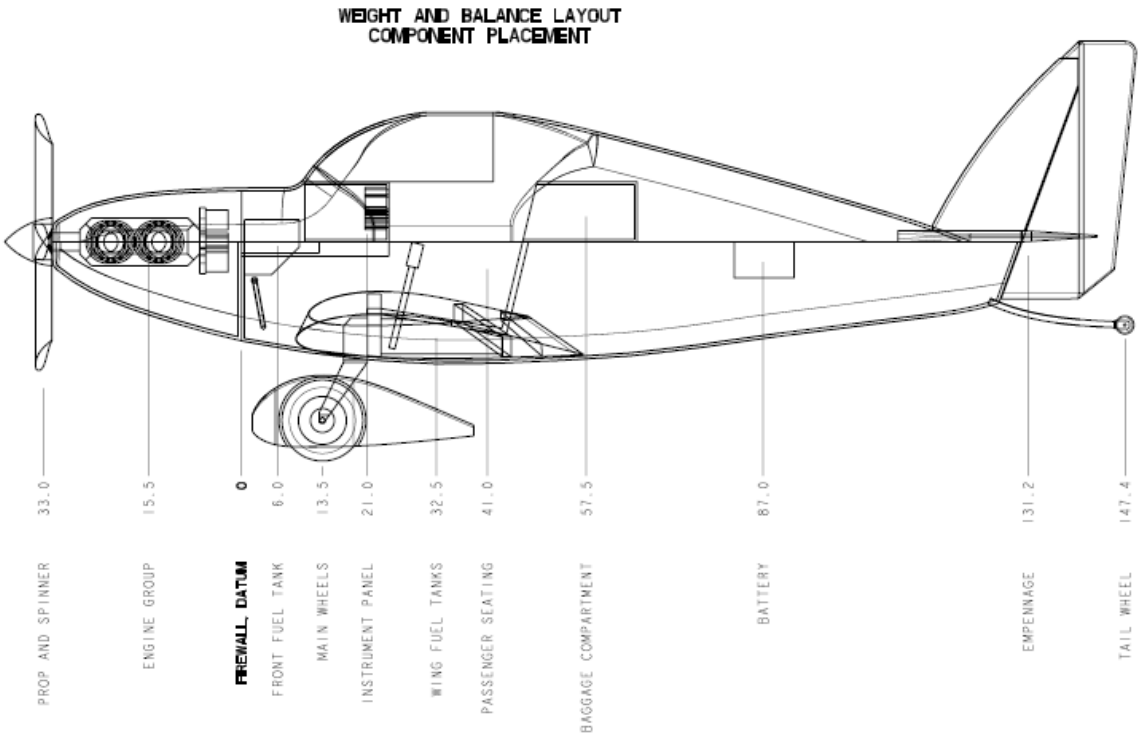

Figure 21: Locations of Major Components for Weight and Balance

Many component weights and locations are known, since they are on hand, such as the engine, starter, magnetos, fuel tanks, engine mount, instruments, and the canopy. However, the weight of the outer wing sections is not known, and added weight is required for fiberglass lay-up. Estimations for these are included in the airframe section of the tabulation.

The methodology of the tabulation is as follows. The firewall is chosen as the datum, with a negative value for locations forward of the firewall, and a positive value for locations aft of the firewall. The engine group weight and arm location are determined. The airframe as weighed on the scales is added to the components not yet installed, including the engine group. The empty weight, *EW*, and center of gravity, CG, locations are calculated. The operating empty weight, *OEW*, is equal to the empty weight plus trapped fuel, oil, and pilot. Take off weight, *TOW*, includes passenger, fuel, and baggage.

It is also required to know the forward extreme CG and the aft extreme CG. These are computed from loading the aircraft in such a manner as to move the CG to the limits. For the forward extreme CG, *OEW* is complemented with components that are forward of the *OEW* CG. In this case, full front fuel is added. For the aft extreme CG, *OEW* is complemented with passenger, full wing fuel, and baggage (with no front fuel).

Weight and Balance Sheet for Modified KR2, 21 Nov 2006					
Datum is the fire wall					
Note: Rear of fire wall is Positive and Forward is Negative. All calculations performed in metric and then converted to inches and pounds.					
	Arm (mm)	Weight (kg)	Moment	Arm (in)	Weight (lb)
Engine Group					
Continental 85 HP engine	-419	97.1	-40684.9	-16.50	214.07
Engine mount	-140	1.5	-210	-5.51	3.31
Starter motor	-101	6.5	-656.5	-3.98	14.33
Magnetos	-101	5	-505	-3.98	11.02
Propeller and Spinner	-838	4	-3352	-32.99	8.82
Total Engine Group Weight		**114.1**	**-45408.4**		**251.54**
Center of Gravity	**-398**			**-15.67**	
Airframe					
Mains (Boat Weight, measured)	343	64.4	22089.2	13.50	141.98
Tail (Boat Weight, measured)	3744	12.7	47549	147.40	28.00
Instrument Panel (not fitted)	533	3.5	1866	20.98	7.72
Battery (not fitted)	2210	6.0	13260	87.01	13.23
Engine Group (from above, not fitted)	-398	114.1	-45408	-15.67	251.54
Front Fuel Tank, 14.6 gal (not fitted)	152	1.5	228	5.98	3.31
Wing Fuel Tanks, 14.1 gal (not fitted)	826	3.0	2478	32.52	6.61
Wing Group (not fitted)	762	25.0	19050	30.00	55.12
Canopy Group (not fitted)	940	12.0	11280	37.01	26.46
Empennage Group (not fitted)	3332	8.0	26656	131.18	17.64
Empty Weight		**250.2**	**99047**		**551.59**
Center of Gravity	**396**			**15.59**	
Trapped Fuel Front (1 gal)	152	2.8	424	5.98	6.15
Trapped Fuel Wings (2 gal)	826	5.6	4609	32.52	12.30
Oil (.5 gal)	-419	1.7	-696	-16.50	3.66
Pilot	1041	80.0	83280	40.98	176.37
Operating Empty Weight		**340.2**	**186665**		**750.07**
Center of Gravity	**549**			**21.60**	
Front Fuel (13.6 gal)	152	37.9	5767	5.98	83.64
Wing Fuel (12.1 gal)	826	33.8	27880	32.52	74.41
Passenger	1041	60.0	62460	40.98	132.28
Baggage	1461	15.0	21915	57.52	33.07
Take Off Weight (Gross Weight)		**486.9**	**304687**		**1073.47**
Center of Gravity	**626**			**24.64**	
Front Fuel (13.6 gal)	152	37.9	5767	5.98	83.64
Wing Fuel (12.1 gal)	826	0.0	0	32.52	0.00
Passenger	1041	0.0	0	40.98	0.00
Baggage	1461	0.0	0	57.52	0.00
Forward Extreme Loading		**378.2**	**192431**		**833.71**
Center of Gravity	**509**			**20.03**	
Front Fuel (13.6 gal)	152	0.0	0	5.98	0.00
Wing Fuel (12.1 gal)	826	33.8	27919	32.52	74.52
Passenger	1041	60.0	62460	40.98	132.28
Baggage	1461	15.0	21915	57.52	33.07
Aft Extreme Loading		**449.0**	**298959**		**989.93**
Center of Gravity	**666**			**26.21**	

Empty Weight	250.2 kg	551.59 lb
Operating Empty Weight	340.2 kg	750.07 lb
Maximum Take Off Weight	486.9 kg	1073.47 lb
Forward Extreme CG	509 mm	20.03 in
Aft Extreme CG	666 mm	26.21 in
CG Range	157 mm	6.18 in
Main Wheel Arm	343 mm	13.5 in
Mean Geometric Chord Leading Edge	254 mm	10.0 in
Mean Geometric Chord Trailing Edge	1367 mm	53.82 in

Figure 22: Weight and Balance Calculations and Summary

The weight and balance analysis yields several interesting results. The range for CG is 6.18 inches, from 20.03 inches to 26.21 inches from the firewall. It is valuable also to consider the location of the CG range in terms of fraction of mean geometric chord as show in the Excursion Diagram, Figure 23. Here the CG range is from 0.23 to 0.37 fraction of mean geometric chord. This will be useful for determining the static margin.

Take off weight is 1073 lb., which is 173 lb. more than the 900 lb. as recommended for the unmodified KR-2, but comparable to other KR-2's with modifications. As mentioned earlier, the structural integrity of the design has been increased to accommodate a greater gross weight, but a complete structural analysis should certainly be performed. Rand Engineering notes that the KR-2 is "a six G airplane at a gross weight of 900 lb. and a five G airplane at 1050 pounds."[9] Also, the useful load is gross weight minus *EW*. Due to the large fuel reserves, the useful load is 1073 lb. - 552 lb. = 521 lb.

[9] "Tom Crawford's KR-2," *Sport Aviation*, February 1999, p. 47.

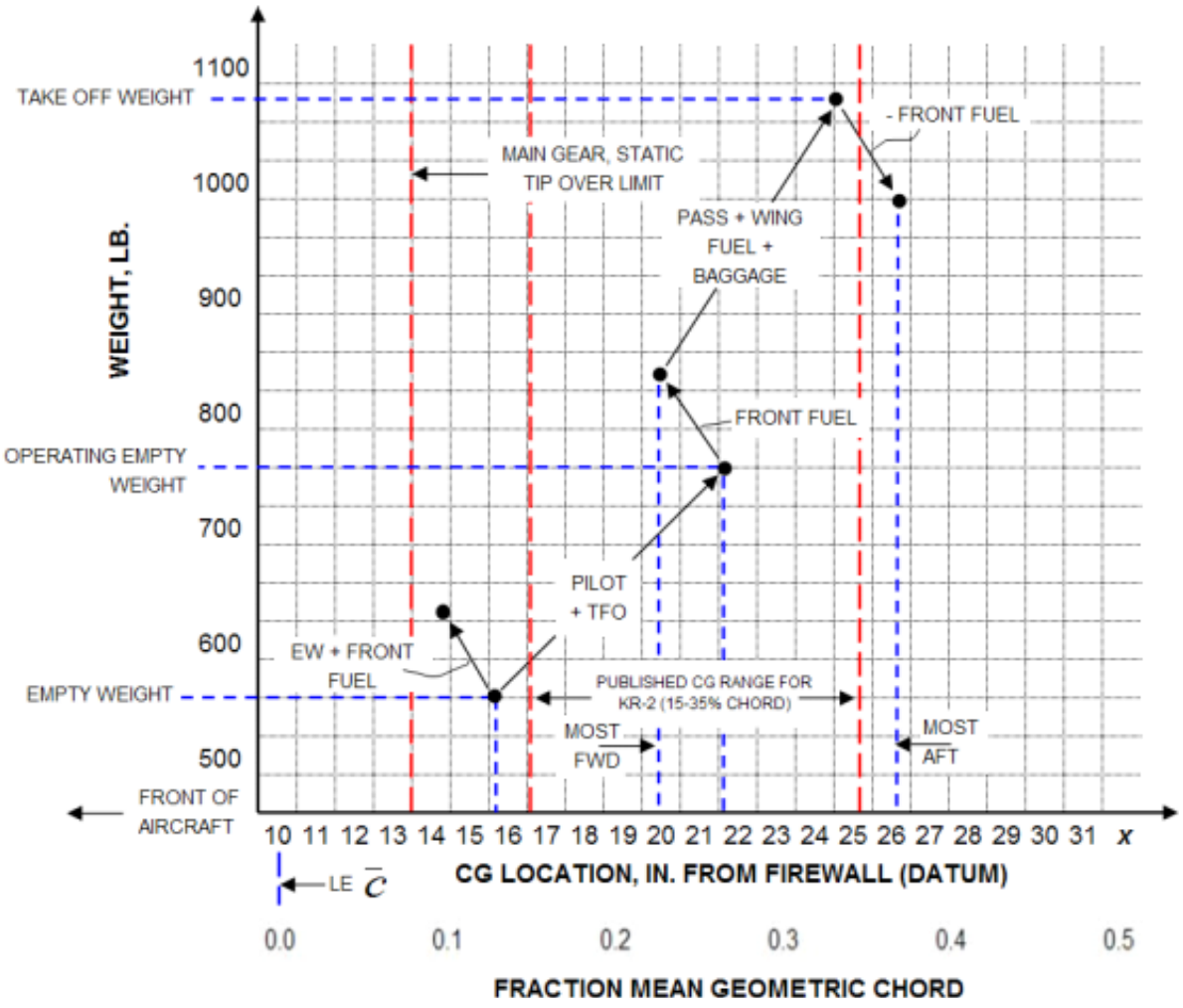

Figure 23: Weight and Balance Excursion Diagram

One suggestion for reducing the weight of the aircraft is to remove the electrical system. Although this will require hand-cranking the propeller to get the engine started, the battery and the starter can be removed for a weight savings of 30 lb.

The main landing gear location is noted on the excursion diagram. Although the main gear has been moved forward on our modified design, it is still possible to load the aircraft such that the CG is precariously close to the main gear. If fuel is added to the front tanks without any fuel in the wing tanks, the CG is less than 1 inch from the main gear. However, all cases with pilot on board move the CG more than 6 inches away from the main gear.

This famously pitch sensitive aircraft requires extra care in choosing a proper center of gravity location. Rand Engineering has a recommended CG range for the KR-2 of 15-35% of wing chord, or 16.5 – 25.0 inches from the firewall. As seen in the excursion diagram, the most aft loading condition results in the CG moving aft of the recommended range. This condition occurs as noted in the table as the gross weight, or take-off weight, subtracting the front fuel. A solution to assuring this case never occurs is to have the wing tanks feed the front fuel tank, keeping the front fuel tank near full until the wing tanks are depleted. Since the recommended range is for a standard KR-2 and not for this modified aircraft, this recommended range for CG may not apply exactly. A look at the moment loads relating the center of lift to the center of gravity will determine if there is a different range for our aircraft.

The static margin is a function of CG and the neutral point, and is a strong indicator of the static longitudinal stability of the aircraft. The neutral point, h_n, is the point at which the moment coefficient for the aircraft does not change with a change in angle of attack. It is always desired to have the center of gravity location, h, forward of the neutral point in order to maintain static longitudinal stability. The static margin is simply the distance between the center of gravity and the neutral point in percent mean chord. Per the following equation, static margin should always be positive:

$$\text{static margin} = h_n - h$$

Reference the following figures for symbols used the subsequent calculations.

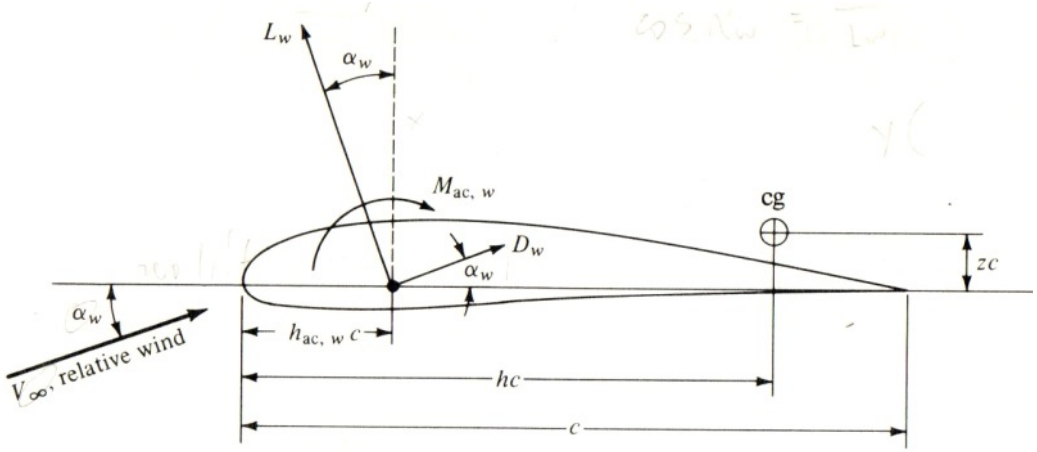

Figure 24: Airfoil Nomenclature and Geometry[10]

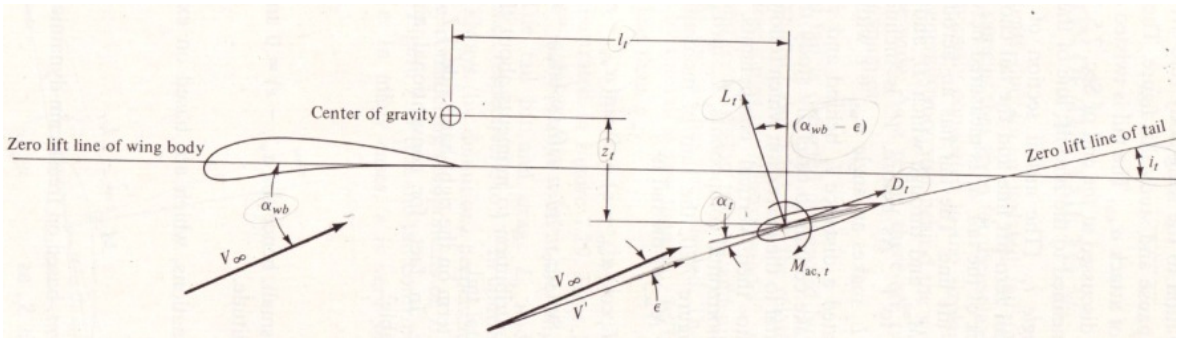

Figure 25: Geometry of Wing-Tail Combination[11]

A good rule of thumb is to have a 10% static margin. An approximate calculation of the neutral point follows. First, the CG location is expressed in terms of fraction of mean

[10] Anderson, John. Introduction to Flight. p. 357.
[11] Anderson, John. Introduction to Flight. p. 362.

chord. The reference unit for fraction of mean chord is on the *x*-axis of the excursion diagram. Using the locations of the CG in the weight and balance table, Figure 22, the location h of the CG for three cases is calculated:

$$h_{AFT} = \frac{h_{AFT}c}{c} = \left(\frac{26.2 - 10.0}{48} \right) = 0.33$$

$$h_{FWD} = \frac{h_{FWD}c}{c} = \left(\frac{20.0 - 10.0}{48} \right) = 0.21$$

$$h_{TO} = \frac{h_{TO}c}{c} = \left(\frac{24.6 - 10.0}{48} \right) = 0.31$$

The neutral point is effectively the aerodynamic center of the entire aircraft, and it is aft of the aerodynamic center of the wing as a function of the location and characteristics of the tail section.

$$h_n = h_{ac,wb} + V_H \frac{a_t}{a} \left(1 - \frac{\partial \varepsilon}{\partial \alpha} \right) \qquad \textbf{Equation 2}$$

where:

- $h_{ac,wb}$ is the location for the aerodynamic center for the wing body.

  $h_{ac,wb} = 0.25$ by approximating the location at the quarter chord location.

- V_H is the tail volume ratio.

  $$V_H = \frac{l_t S_t}{cS}$$

  and:

  - l_t as in Figure 25. $l_t = 107.0 \text{ in}$ from geometry
  - $S_t = 1760 \text{ in}^2$, the horizontal stabilizer area
  - $c = 43.8 \text{ in}$, the wing mean chord
  - $S = 12440 \text{ in}$, the wing area

  $$V_H = \frac{107 \times 1760}{43.8 \times 12440} = 0.346$$

- a_t is the lift curve slope of the horizontal stabilizer. Assuming a NACA 0009 symmetrical airfoil is used for the tail, $a_t = 6.45 \text{ rad}^{-1}$.

- a is the lift curve slope of the wing. As previously calculated in Chapter VIII, $a = 5.86 \text{ rad}^{-1}$.
- $\frac{\partial \varepsilon}{\partial \alpha}$ is the change in downwash per change in angle of attack for the tail. This data is usually obtained from wind tunnel testing. For this case we assume it is a typical value of 0.35.[12] Hence:

$$h_n = 0.25 + (0.346)\left(\frac{6.445}{5.86}\right)(1 - 0.35)$$

$$h_n = 0.497 \approx .50$$

The static margin for most forward loading, most aft loading, and for take-off weight is calculated:

Aft Loading CG: $\text{static margin} = h_n - h_{CG,AFT} = 0.497 - 0.33 = 0.17$

Forward Loading CG: $\text{static margin} = h_n - h_{CG,FWD} = 0.497 - 0.210 = 0.29$

Take Off CG: $\text{static margin} = h_n - h_{CG,TO} = 0.497 - 0.310 = 0.18$

Note that the static margin in all three cases is positive. The results indicate that our modified KR-2 has a good longitudinal static stability. However, many assumptions were made in this preliminary estimation, and a more thorough study is recommended prior to final layout of components.

[12] Anderson, John. Introduction to Flight. From example on page 365.

VII. Airfoil Lift and Drag

A complete two-dimensional analysis of the airfoil chosen for use on the project aircraft is performed here. A look at pressure distribution, the C_L-α curve, and the drag polar for cruise condition is presented. A comparison is made with a new airfoil designed for the KR-2S.

A. The RAF48 – Specified Airfoil

The airfoil specified for the KR-2 is the RAF48, originating from the 1930's in Britain from the Royal Aircraft Factory. The RAF series of airfoils were used on WWI aircraft.[13] For a modern homebuilt aircraft to specify such an old airfoil is perplexing, since much development on more efficient airfoils for general aviation has been made since then. Therefore, research into alternate airfoils for this project is worthy of some consideration. A look at an alternate airfoil will follow. First we take a look at the RAF48. Coordinates were obtained for the RAF48 airfoil from a database, and the profile is shown in Figure 26.

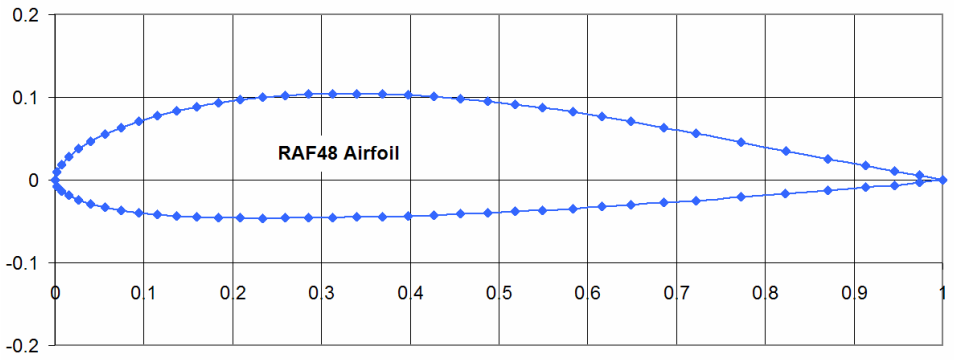

Figure 26: RAF48 Airfoil

Airfoil parameters, some of which will be used in subsequent analysis, are obtained with the software package *Xfoil* for unit chord as shown in Figure 27. Note the leading edge radius of 0.018. This is a 15% airfoil with maximum thickness at x/c=.312. Maximum camber is .029 at x/c=.368.

[13] Anderson, John. Introduction to Flight. Page 231.

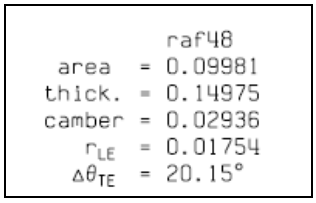

Figure 27: RAF48 Airfoil Parameters Plotted in Xfoil

Xfoil features menu-based airfoil analysis tools for both viscous and inviscid solutions. Inviscid solutions are obtained utilizing a linear vorticity stream function panel method. The viscous solution "is strongly interacted with the incompressible flow via the surface transpiration model."[14] Although the menu driven functionality is cumbersome to learn, results can be achieved quickly once proficiency is gained.

The condition used for the airfoil analysis is an estimated cruise condition of 190 mph at 6000 feet elevation. Reynolds number is here computed for Standard Atmosphere. *Xfoil* computes results for a unit chord length; hence the characteristic length L is removed for use in the software.

$$\mathrm{Re} = \frac{\rho_\infty V_\infty L}{\mu} = \frac{\left(1.021\frac{kg}{m^3}\right)\left(84.94\frac{m}{s}\right)(1.143m)}{1.717\text{x}10^{-5}\frac{N\cdot s}{m^2}} \qquad \textbf{Equation 3}$$

$$\mathrm{Re} = 5{,}773{,}000$$

$$\mathrm{Re}_{Xfoil} = \frac{V_\infty}{\nu} = \frac{84.94\frac{m}{s}}{1.682\text{x}10^{-5}\frac{m^2}{s}}$$

$$\mathrm{Re}_{Xfoil} = 5{,}050{,}000$$

[14] *Xfoil 6.9* User Guide, from *Xfoil* Subsonic Airfoil Development System, http://web.mit.edu/drela/Public/web/xfoil/ .

The Mach number at cruise speed of 190 mph is 0.25, also needed for the analysis. A sequence of angle of attacks is prescribed and Xfoil, and now the C_L-α curve is plotted in Figure 28. Here we obtain the maximum lift coefficient, $C_{L,\,MAX}$, the zero-lift angle of attack, $\alpha_{CL=0}$, the zero-alpha lift coefficient, $C_{L,\alpha=0}$, angle of attack for stall onset at $C_{L,\,MAX}$, and the lift curve slope, m. These parameters are used in the formulation of the wing list distribution in the next chapter.

$C_{L,\,MAX}$=1.62
$\alpha_{CL=0}$=-2.5°
$C_{L,\,\alpha=0}$=0.28
$\alpha_{CL\,MAX}$=17.3°
m= 6.0 rad^{-1}

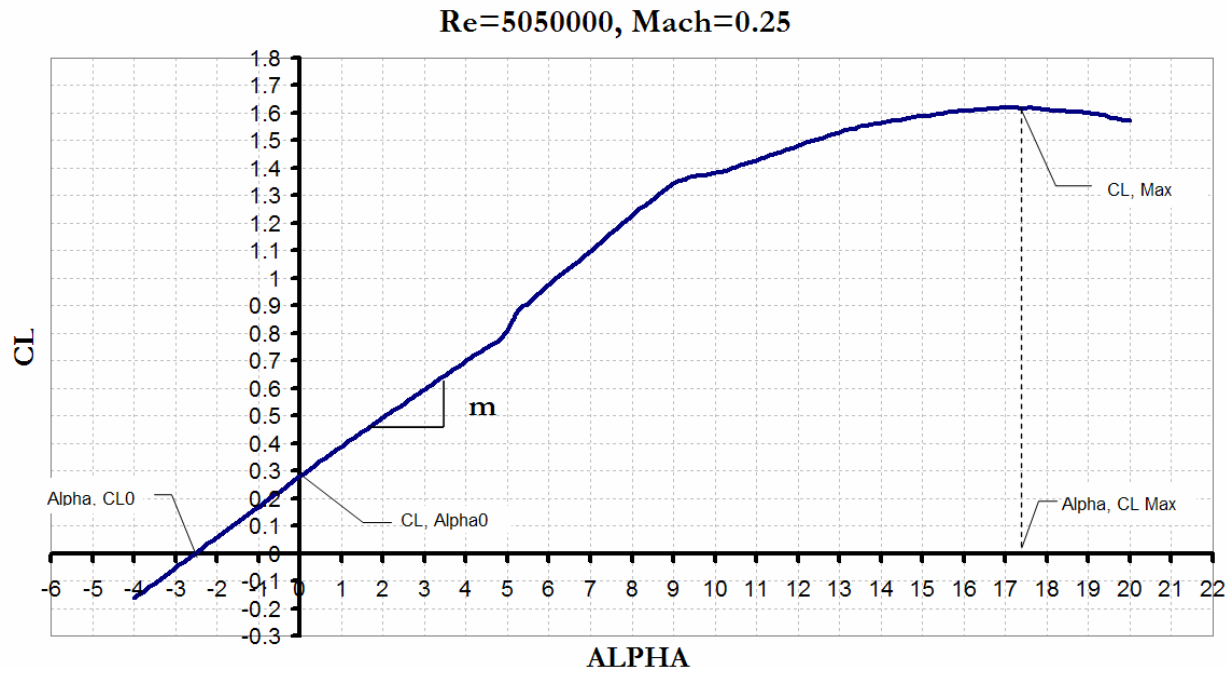

Figure 28: RAF48 CL-Alpha Curve – plotted with XFOIL

B. The AS5046 – An Alternative Airfoil Developed for the KR-2S

A comparison is here made to determine if the specified airfoil for the modified KR-2 could be improved upon. An alternate airfoil for use on the KR-2S was developed in 1998 by Dr. Gopalatathnam by the request of Mark Langford with improved speed performance and efficiency.[15] The AS504X is a low camber airfoil with favorable performance over the RAF48. For a new construction, an AS5048 (18% airfoil) could be used at the root, tapering to an AS5045 (15% airfoil) at the tip. This allows for increased spar strength and extra fuel tank capacity. For a project which already has the stock wing spars constructed, as is the case for this project, an AS5046 (16% airfoil) is recommended. A profile comparison is shown in Figure 29. The AS5046 has a supercritical-like shape with a flatter upper surface and an increase in camber in the aft section. A plot of the C_L-α curve comparing the AS5046 to the RAF48 is shown in Figure 30. With a higher $C_{L,MAX}$ of 1.77, it is predicted that a higher stall speed would be obtained, and this has added benefits for maneuvering. However, looking at the comparison of drag polars in Figure 31, the drag is higher for the AS5046 in the C_L range from 0.5 to 1.4, which is about half of the operating range for a general aviation aircraft. The computation of additional performance parameters for the AS5046 will be bypassed, as the continued analysis of the modified KR-2 is based on the RAF48 airfoil.

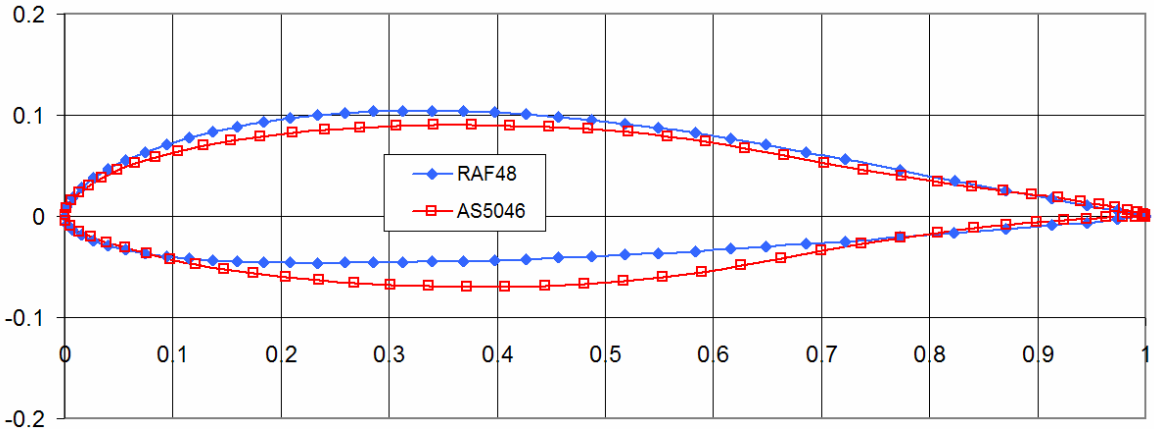

Figure 29: Profile Comparison

[15] The "New" KR-2S Airfoil, http://home.hiwaay.net/~langford/airfoil.html.

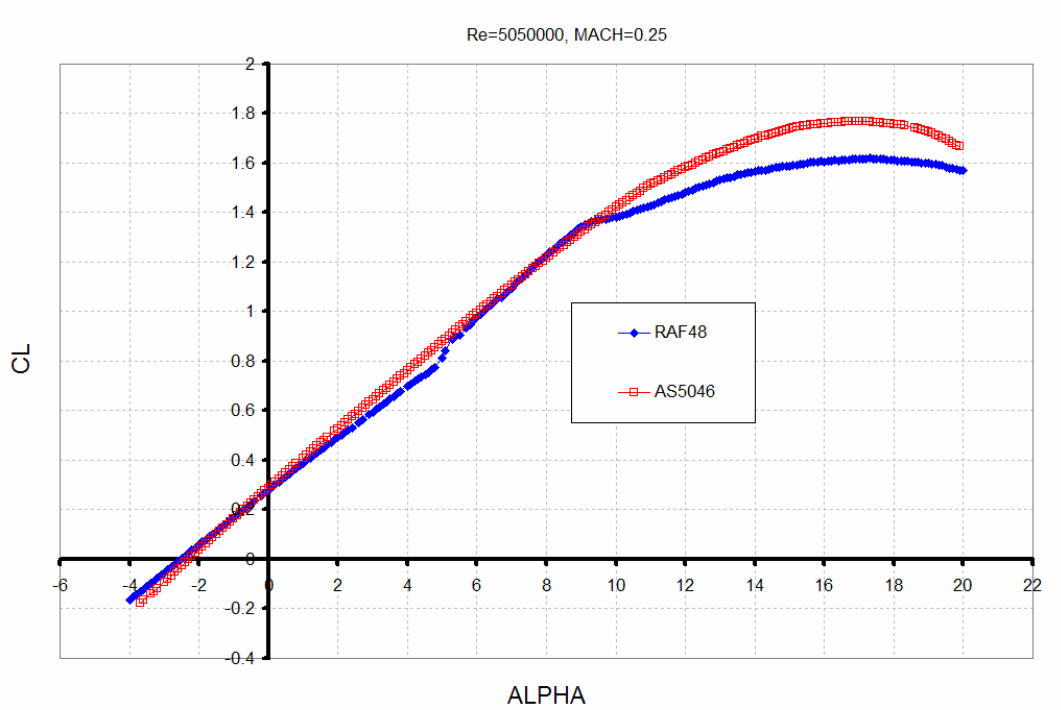

Figure 30: CL-α Curve Comparison – plotted with *Xfoil*

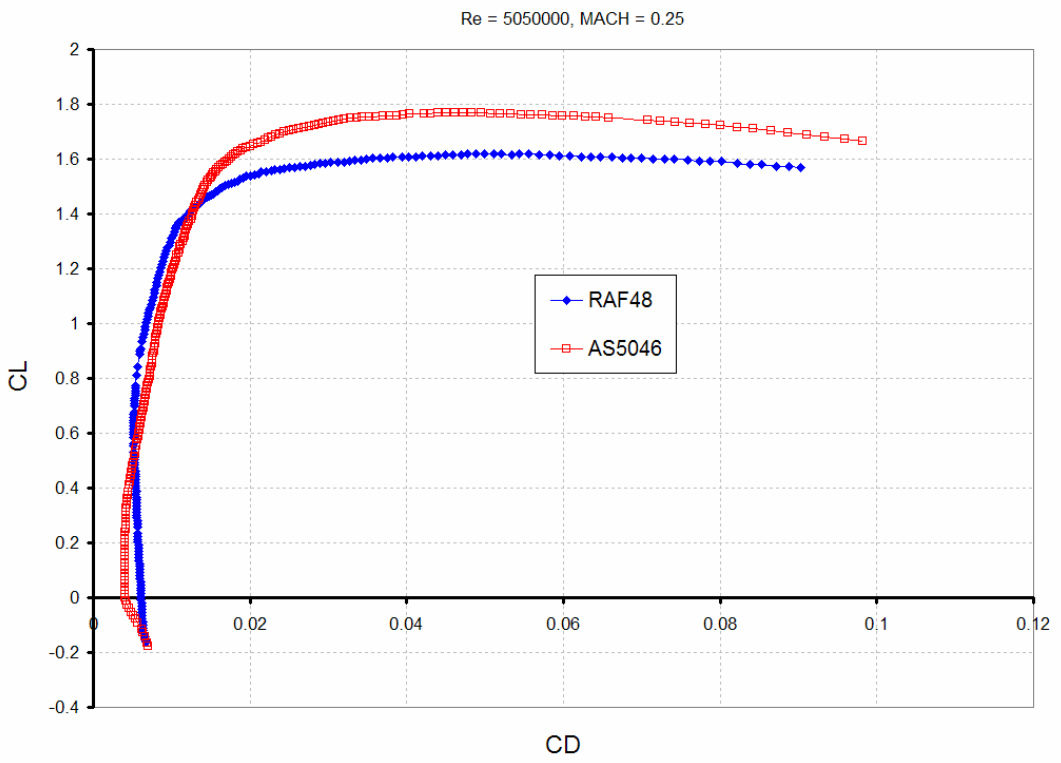

Figure 31: Drag Polar Comparison – plotted with *Xfoil*

VIII. Wing Lift and Drag

A. Derivation

A span-wise lift distribution of the wing is determined from the known characteristics of the airfoil from the previous chapter and the wing planform. Regular wing sections such as straight wing, constant taper or elliptical planforms have elegant simple equations for the determination of the wing lift distribution. However, the KR-2 has a complicated non-uniform taper and non-uniform twist in the planform. This was part of the design because the aircraft has removable outer wing sections. The wing is straight until the removable section. The outer sections have a linear change in both chord length and twist. A method is presented here for the determination of span-wise wing lift distribution for non-uniform taper and twist using a derivation that combines the trailing vortices theory and potential flow theory, as derived by Herman Glauert.[16] The end result yields coefficient of lift as a function of span-wise wing station, $C_L = f(x)$, which is valid for the linear region of the $C_L - \alpha$ curve.

For a vortex, the circulation Γ is $2\pi\kappa$, where κ is the strength of the vortex. Hence, the lift per unit length of a wing is as follows per the Kutta-Joukowski Theorem, valid for inviscid, incompressible flow.

$$L' = 2\pi\kappa_0\rho_\infty V_\infty \qquad \textbf{Equation 4}$$

Glauert considers the set of variables in Figure 32 for the derivation, where $x = s\cos\phi$, $b = s\cos\theta$ and s is half of the wingspan. "ϕ and θ vary from 0 to π as x and b vary from s to $-s$."[17] From Trailing Vortices Theory, the vortex strength is arrived at as a function of the local angle of attack and chord length as a Fourier series, *exactly* applicable to our wing that has non-uniform twist and taper. This method applies for inviscid, incompressible potential flow. Vortex strength κ will be phased out of this relationship as lift coefficient is solved for.

$$\kappa_0 = \sum A_n \sin n\phi \left\{ sV_\infty + \frac{\pi}{2} \cdot \frac{\partial \kappa_0}{\partial \alpha_o} \cdot \frac{n}{\sin\phi} \right\} \qquad \textbf{Equation 5}$$

[16] Bairstow, Leonard. Applied Aerodynamics, Second Edition. Chapter 8.
[17] Bairstow, Leonard. Applied Aerodynamics, Second Edition. Page 437.

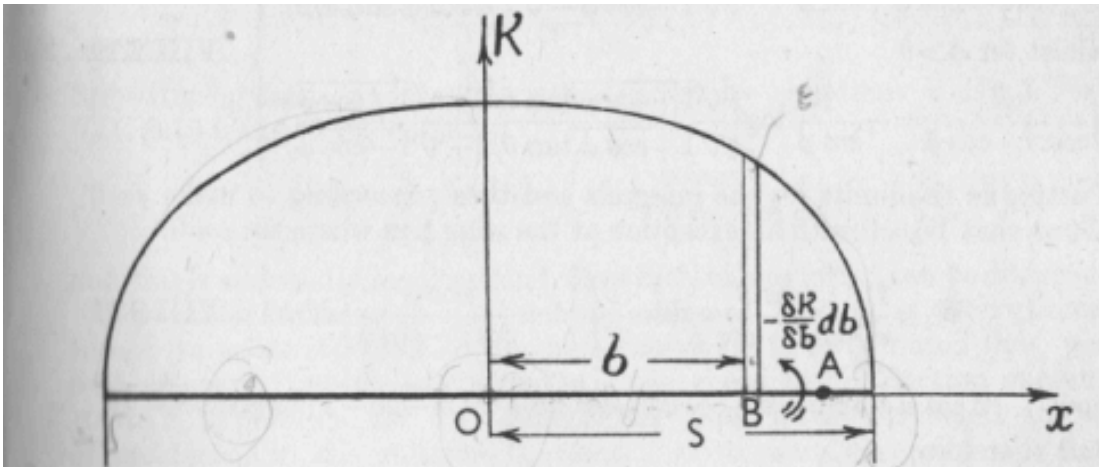

Figure 32: Vortex Strength along Wingpsan[18]

Lift per unit length is also defined as $L' = 1/2\rho V_\infty{}^2 c_0 C_L$. Combining this with Equation 4 yields

$$2\pi\kappa_0 \rho V_\infty = \frac{1}{2}\rho V_\infty{}^2 c_0 C_L \ . \qquad \textbf{Equation 6}$$

Solving for C_L:

$$C_L = \frac{4\pi\kappa_0}{V_\infty c_0} \qquad \textbf{Equation 7}$$

Solving for κ_0:

$$\kappa_0 = \frac{C_L V_\infty c_0}{4\pi} \qquad \textbf{Equation 8}$$

[18] Bairstow, Leonard. Applied Aerodynamics, Second Edition. Page 437

Substituting for κ in Equation 4:

$$\frac{C_L V_\infty c_0}{4\pi} = \sum A_n \sin n\phi \left\{ sV_\infty + \frac{\pi}{2} \cdot \frac{\partial \kappa_0}{\partial \alpha_o} \cdot \frac{n}{\sin \phi} \right\} \qquad \textbf{Equation 9}$$

From the lift curve slope:

$$C_{L_0} = m\alpha_o \qquad \textbf{Equation 10}$$

where $\alpha_0 = \text{effective angle of attack} = \alpha - \alpha_{CL=0}$ as defined by the figure below. The assumption is made that the fuselage has no incidence angle to the free stream velocity in cruise configuration.

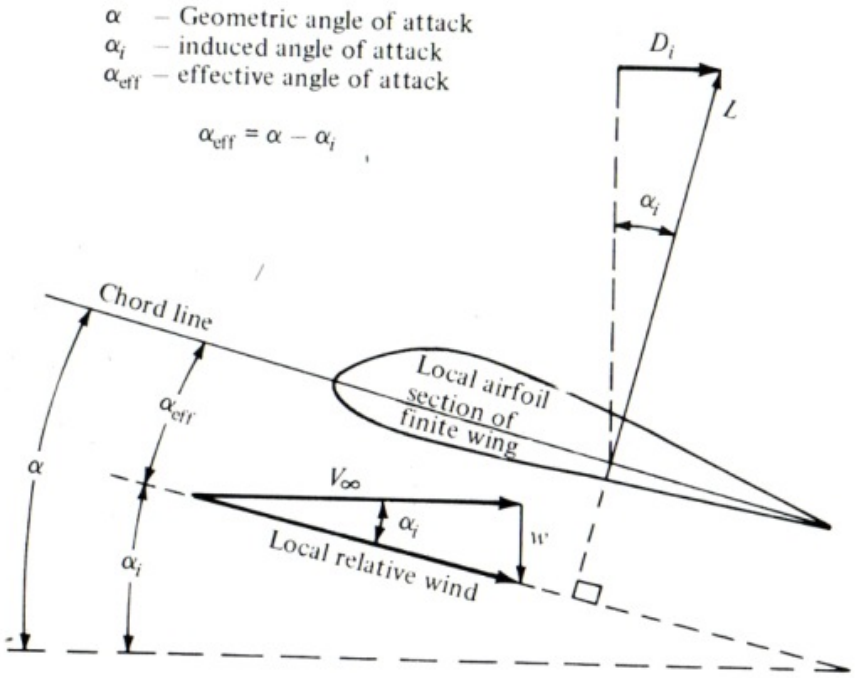

Figure 33: Effect of Downwash on the Local Flow over a Local Airfoil Section of a Finite Wing[19]

Substituting for C_L in Equation 4:

$$\frac{m\alpha_o V_\infty c_0}{4\pi} = \sum A_n \sin n\phi \left\{ sV_\infty + \frac{\pi}{2} \cdot \frac{\partial \kappa_0}{\partial \alpha_o} \cdot \frac{n}{\sin \phi} \right\} \qquad \textbf{Equation 11}$$

[19] Anderson, John. Fundamentals of Aerodynamics. p. 318.

Combining Equations 6 and 9 then solve for κ_0 / α_0:

$$C_{L_0} = m\alpha_o = \frac{4\pi\kappa_0}{V_\infty c_0} \qquad \textbf{Equation 12}$$

$$\frac{\kappa_0}{\alpha_o} = \frac{mV_\infty c_0}{4\pi} \text{ and } \kappa \text{ is proportional to } \alpha_o \qquad \textbf{Equation 13}$$

in the linear region of the $C_L - \alpha$ curve. Then it follows that

$$\frac{\kappa_0}{sV_\infty} \equiv \frac{mc_0\alpha_o}{4\pi s} = \sum A_n \sin n\phi \left\{ 1 + \frac{mc_0}{8s} \cdot \frac{n}{\sin\phi} \right\} \qquad \textbf{Equation 14}$$

and

$$\frac{mc_0\alpha_o}{4\pi s} = \sum A_n \left(\sin n\phi + \frac{mc_0}{8s} \cdot \frac{\sin(n\phi)n}{\sin\phi} \right). \qquad \textbf{Equation 15}$$

Equation 14 is used to solve for the Fourier coefficients A_n. "Rectangular wings, tapered wings and wings of elliptic plan form are adequately dealt with by four terms."[20]

$$\begin{Bmatrix} \frac{m}{4\pi s}\alpha_{o1}c_{o1} \\ \frac{m}{4\pi s}\alpha_{o3}c_{o3} \\ \frac{m}{4\pi s}\alpha_{o5}c_{o5} \\ \frac{m}{4\pi s}\alpha_{o7}c_{o7} \end{Bmatrix} = \begin{bmatrix} a_{11} & a_{13} & a_{15} & a_{17} \\ a_{31} & a_{33} & a_{35} & a_{37} \\ a_{51} & a_{53} & a_{55} & a_{57} \\ a_{71} & a_{73} & a_{75} & a_{77} \end{bmatrix} \begin{Bmatrix} A_1 \\ A_3 \\ A_5 \\ A_7 \end{Bmatrix} \qquad \textbf{Equation 16}$$

where

$$a_{ij} = \sin(j\phi_i) + \frac{mc_{0i}}{8s} \frac{\sin(j\phi_i)j}{\sin(\phi_i)}. \qquad \textbf{Equation 17}$$

After the coefficients are known, the span-wise lift coefficient can be found with

$$C_{L_\phi} = \frac{4\pi s}{c_\phi} \sum A_n \sin(n\phi). \qquad \textbf{Equation 18}$$

[20] Bairstow, Leonard. Applied Aerodynamics, Second Edition. Page 439.

The total lift of the wing is then determined with

$$C_{L,W} = \frac{2\pi^2 s^2 A_1}{S} \; . \qquad \textbf{Equation 19}$$

and the induced drag is found with

$$C_{Di,W} = \frac{\pi^3 s^2}{S} \sum n A_n{}^2 \; . \qquad \textbf{Equation 20}$$

A program was written in Matlab to solve the matrix for the A_n coefficients and for the resulting lift and drag parameters. The Matlab script *Wing Lift Distribution* is posted in the Appendix. The solution set is solved for varying angle of attack.

The first case is outlined here for level flight, with an effective angle of attack varying from 6.0°at the root to 3.0°at the tip. In this case, solving the matrix yields

$$\begin{aligned} A_1 &= \; 0.0161 \\ A_3 &= -0.0001 \\ A_5 &= \; 0.0015 \\ A_7 &= \; 0.0009 \end{aligned} \; .$$

The local lift coefficients, overall lift coefficient, and induced drag of the wing are obtained, and the wing lift coefficient distribution is tabulated and plotted.

$$C_{L(1,3,5,7)} = \{0.6253, \; .5369, \; 0.3812, \; 0.3240\}$$
$$C_{L,W} = 0.5143$$
$$C_{Di,W} = 0.0138$$

x/s	*i*	*s (in)*	c (in)	*CLϕ*
1.00	8	-142.0	36.00	**0**
0.96	7	-136.3	36.77	**0.324**
0.85	5	-120.7	38.64	**0.381**
0.50	3	-71.0	44.60	**0.537**
0.00	1	0.0	48.00	**0.625**
0.50	3	71.0	44.60	**0.537**
0.85	5	120.7	38.64	**0.381**
0.96	7	136.3	36.77	**0.324**
1.00	8	142.0	36.00	**0**
Wing Lift Coef.			**CLw**	**0.514**
Wing Induced Drag Coef.			**CDiw**	**0.014**

Table 2: Tabulation of Lift Coefficient Distribution for Level Flight

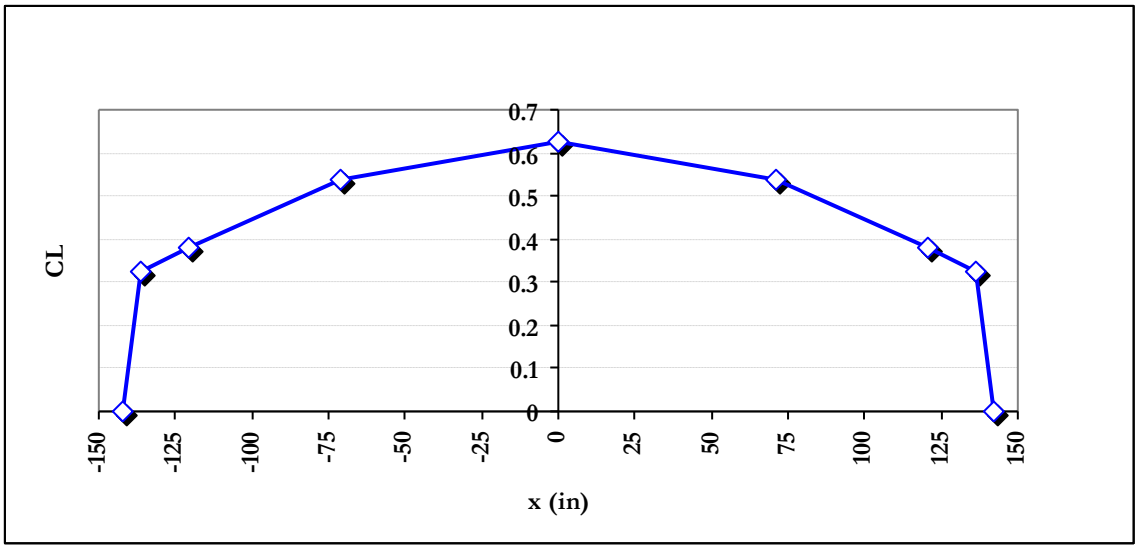

Figure 34: Lift Coefficient Distribution for Level Flight

B. CFD Results

A steady-state computational fluid dynamics analysis has been performed to validate the wing lift distribution calculated with the numerical derivation of Glauert's Trailing Vortices method in the previous chapter.

First, a precise to-scale CAD model of the wing was made in *Pro/Engineer*, complete with the proper airfoil and non-uniform taper and twist. This model was imported to the meshing generator *Gambit*. A rectangular volume was created with dimensions 200' by 200' by 100' as shown in Figure 35. Half of the wingspan was inserted at the incidence angle for level flight. Its volume was subtracted from the rectangular volume to create the computational domain. The wing is attached to the reflection plane, where the viscosity is set to zero. A mesh was generated with approximately two million tetrahedral elements. The elements were specified to be smaller at the surface of the wing. The elements are 1" at the wing surface, 12" at the inlet and the outlet.

Fluent was used for pre-setup, as the solver, and for post-processing. *Fluent* is a finite volume solver that balances the momentum and mass flow at the face of each element in the domain. More specifically, it solves for the turbulent dissipation rate, ε, and for the turbulent kinetic energy, k. Therefore, *Fluent is* commonly referred to as a standard "k-epsilon" solver.

Boundary conditions were setup for cruise condition.

$$V_\infty = 190\ mph$$
$$\rho_\infty = 1.21\ kg/m^3$$
$$P = 81.2\ kPa$$
$$\mu = 1.717\text{x}10^{-5} N \cdot s/m^2$$

Due to the mesh size, the problem is 1.7 gigabytes in size. Hence, to save on computation time, a dividing line was created as shown in Figure 35 such that two computers would be used to solve the problem. One Linux machine with two AMD 64 bit processors was used, and total computation time was several hours.

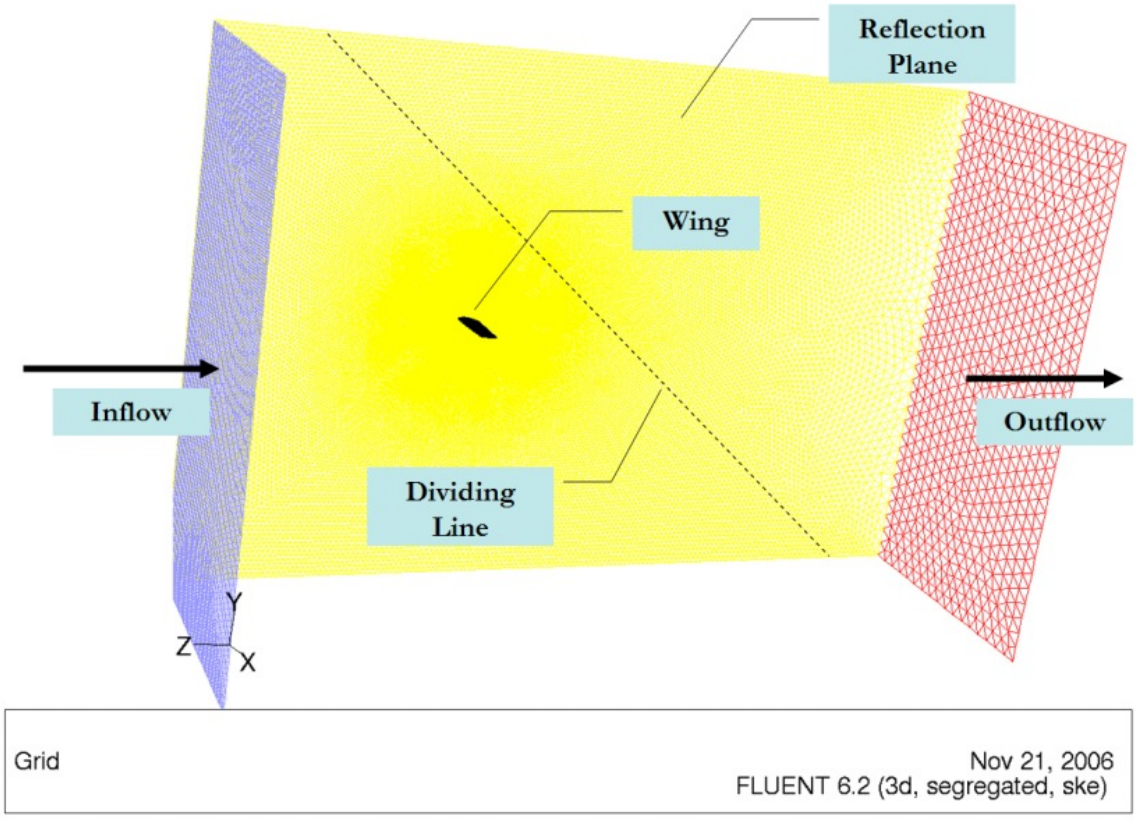

Figure 35: Volume for CFD Analysis

In addition to the dividing line slice, the wing was divided into vertical slices along the chord length for localized computation of lift. In *Gambit*, a one inch wide box was made to slice the domain into sections. Two slices were solved for to see the wing lift distribution. It is desired to later compute additional sections for more detail on the lift distribution. Due to issues with an inconsistency problem with the geometry that was not solved during the slice process, two slices will suffice for this investigation. The first slice is at the reflection plane. The second slice is at the ¼ span location, or 71 inches from the reflection plane.

A detail of the wing mesh is shown in Figure 36, and a view of the 1 inch wing slices is shown in Figure 37.

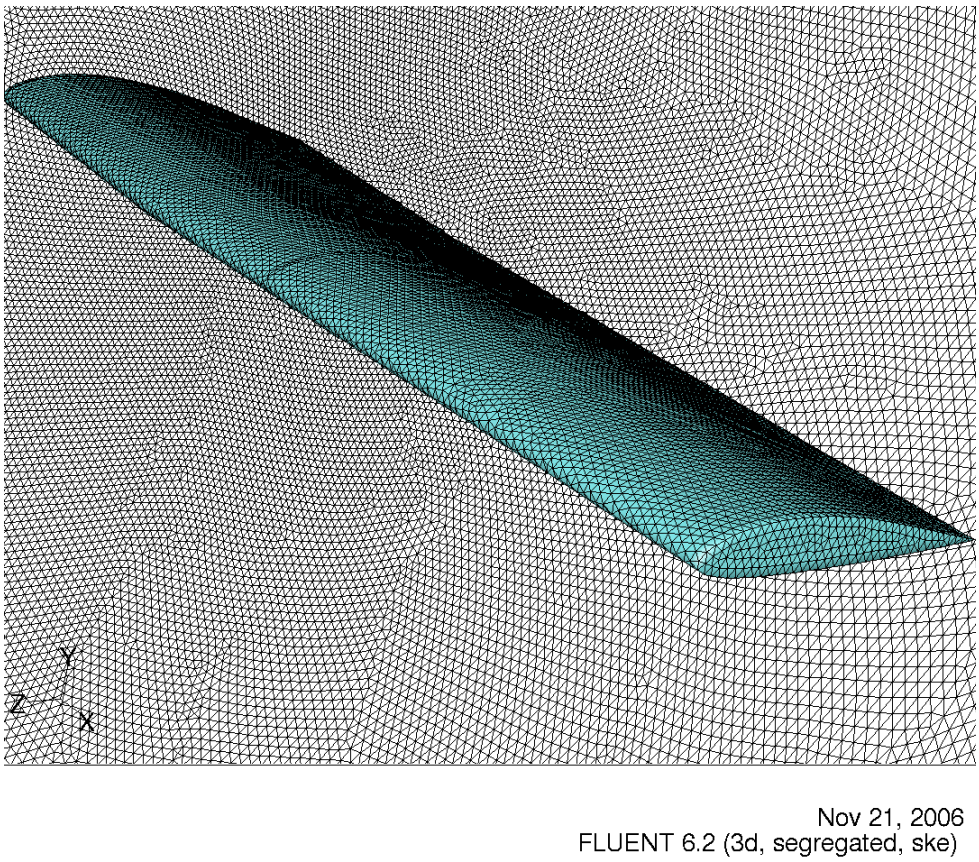

Figure 36: Detail of mesh on wing surface

1" Slices

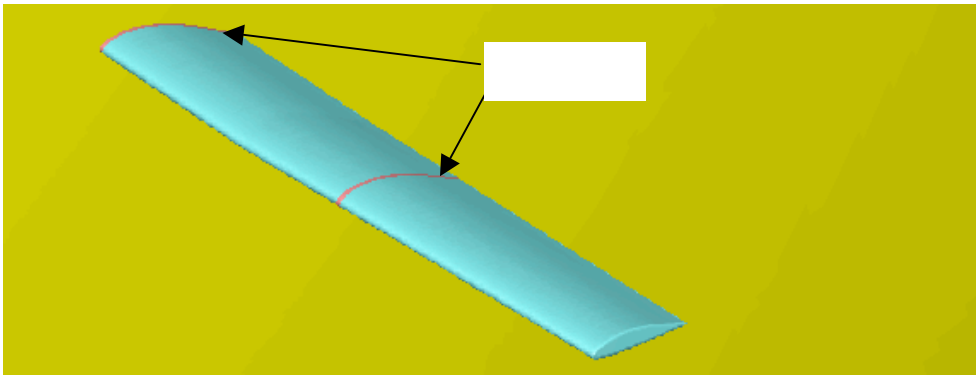

Figure 37: Detail of 1" Wing Sections

A solution was obtained with very low residuals. The solver yields a total y-component of the forces of 8,057 N. Since this is half of the wingspan, the total lift for the wing is 16,114 N. Solving for $C_{L,W}$:

$$C_{L,W} = \frac{L}{1/2 \rho_\infty V_\infty^2 S}$$

$$C_{L,W} = \frac{16{,}114\ N}{1/2(1.021\ kg/m^3)(85\ m/s)^2(8.03\ m^2)} \qquad \textbf{Equation 21}$$

$$C_{L,W} = 0.544$$

This within 5.7% of the result obtained with the Trailing Vortices Theory (TVT) in the previous section.

$$\frac{C_{L,W}(CFD)}{C_{L,W}(TVT)} = \frac{0.544}{0.514} = 5.7\%$$

The lift coefficient is found in the same manner for the slices.

	x/s	*s(in)*	*A(m^2)*	*L(N)*	*CL*
Slice 2	0.5	-71	0.0285	60.97	0.580
Slice 1	0	0	0.0307	71.18	0.629
Slice 2	0.5	71	0.0285	60.97	0.580

Figure 38: Local Lift Coefficient for Wing Slices

These CFD results are plotted against the results from the TVT analysis in Figure 39. The solutions are similar and therefore the CFD results validate the previous results obtained with the derivation obtained using the trailing vortices theory.

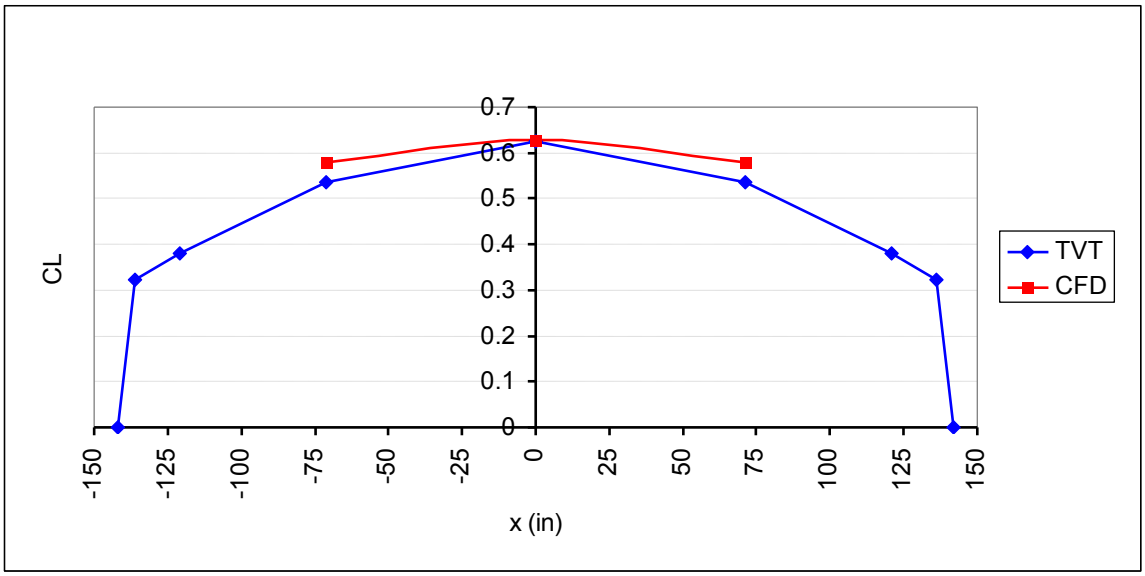

Figure 39: CFD vs. TVT Results for Lift Coefficient Distribution

CFD post processing yields other interesting data that is worth viewing. The plotted stream lines around the tip section of the wing show the vortex formation below:

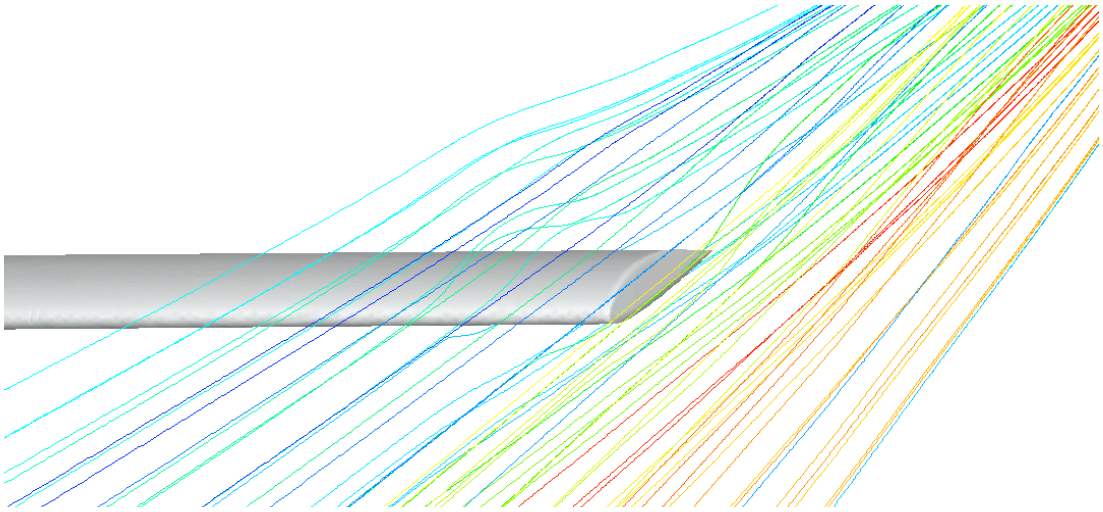

Figure 40: Stream Lines View 1

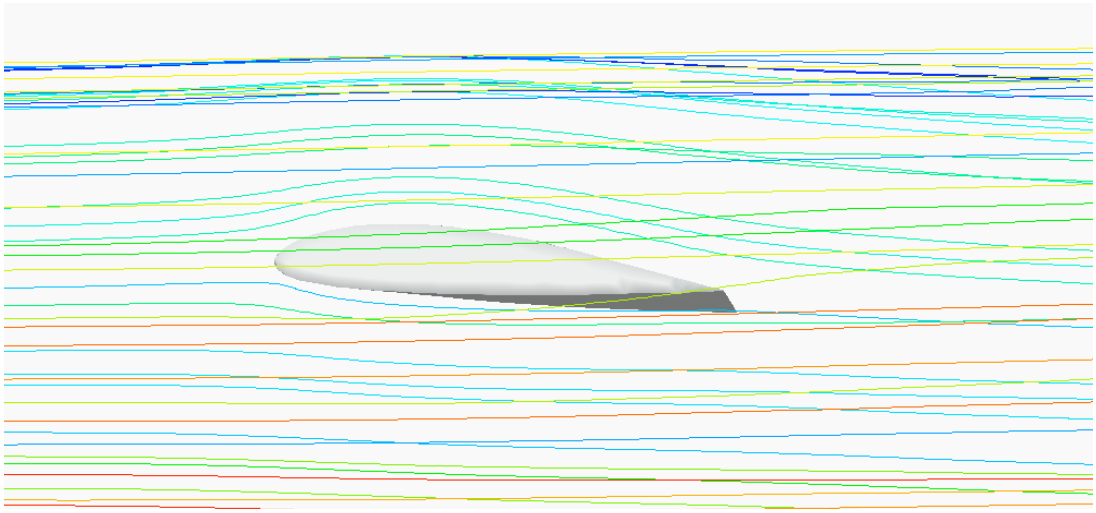

Figure 41: Stream Lines View 1

A view of the static pressure on the wing reveals the lowest pressure at the top surface, where of course the highest velocity also is via the Bernoulli Principle. Another look at the pressure on the reflection plane shows essentially the two-dimensional pressure distribution of the RAF48 airfoil. Note that the air pressure is affected for a notable distance upstream of the wing. The velocity plotted on the reflection plane also shows the effect on free stream velocity. See the following figures.

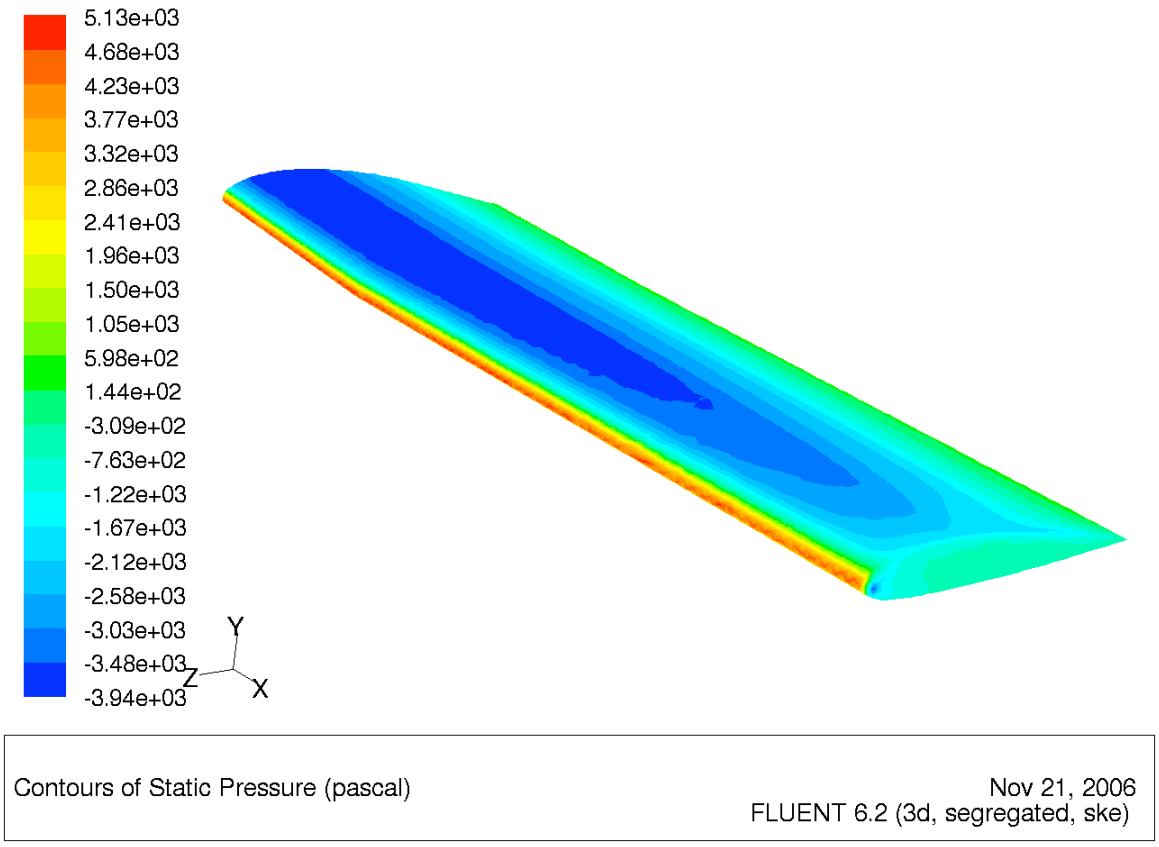

Figure 42: Static Pressure on Top of Wing Surface

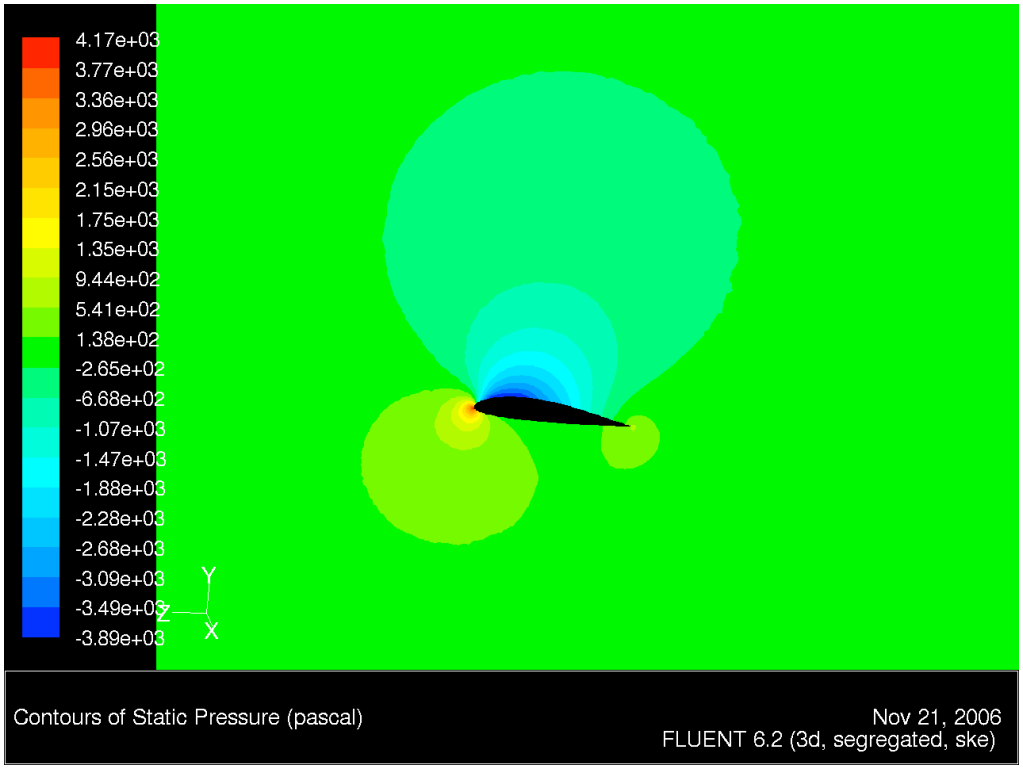

Figure 43: Static Pressure on Reflection Plane

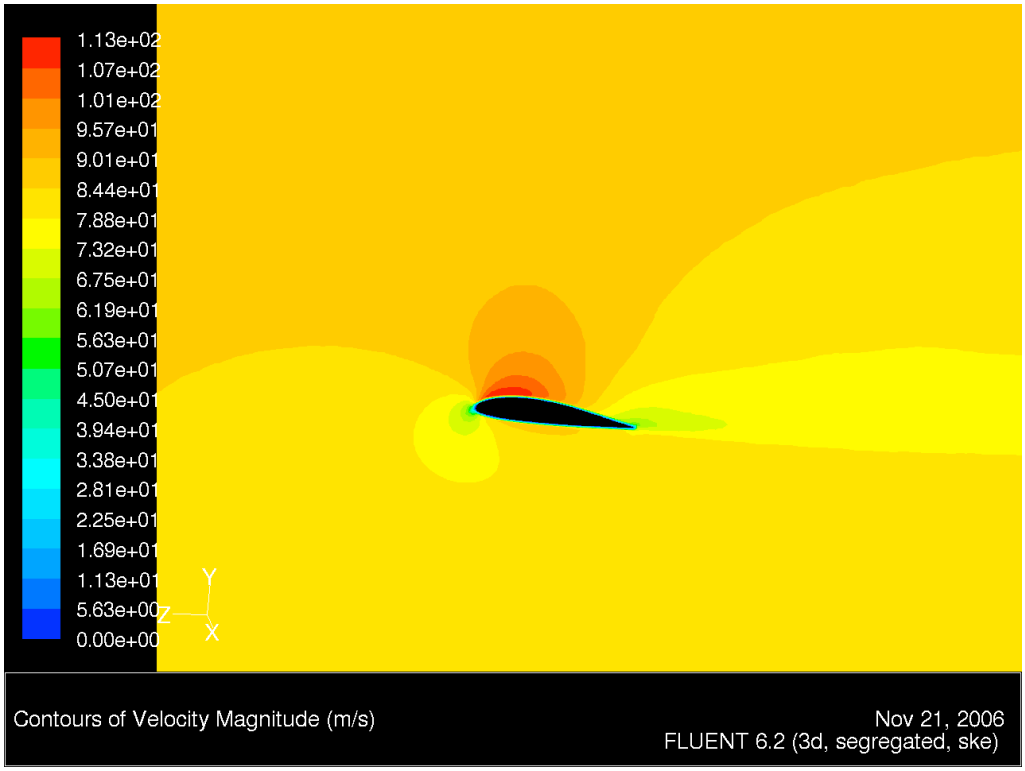

Figure 44: Velocity Magnitude on Reflection Plane

C. Stall Speed Estimation

$C_{L,MAX}$ for the wing is determined by obtaining the local $C_{L,MAX}$ at each wing station for estimated stall speed with *Xfoil* and plotting this against the lift C_L distribution curve. α is increased until the C_L distribution curve crosses the local $C_{L,MAX}$ distribution, and this is where the $C_{L,MAX}$ for the wing occurs. This is the Roskam method is outlined in *Airplne Design Part VI,* Chapter 8.[21]

To determine the local $C_{L,MAX}$, the stall speed of the unmodified KR-2 (52 mph) is taken to find a Reynolds Number for use in *Xfoil* at Standard Atmosphere Sea Level condition. At the wing root:

$$\mathrm{Re} = \frac{\rho_\infty V_\infty c_0}{\mu}$$

$$\mathrm{Re} = \frac{\left(1.225\ kg/m^3\right)\left(23.2\ m/s\right)\left(1.219m\right)}{1.789\mathrm{x}10^{-5} Pa \cdot s} \qquad \textbf{Equation 22}$$

$$\mathrm{Re} = 1{,}940{,}000$$

A plot of the C_L-α curve in *Xfoil* yields the local $C_{L,MAX}$ of 1.55 as shown below.

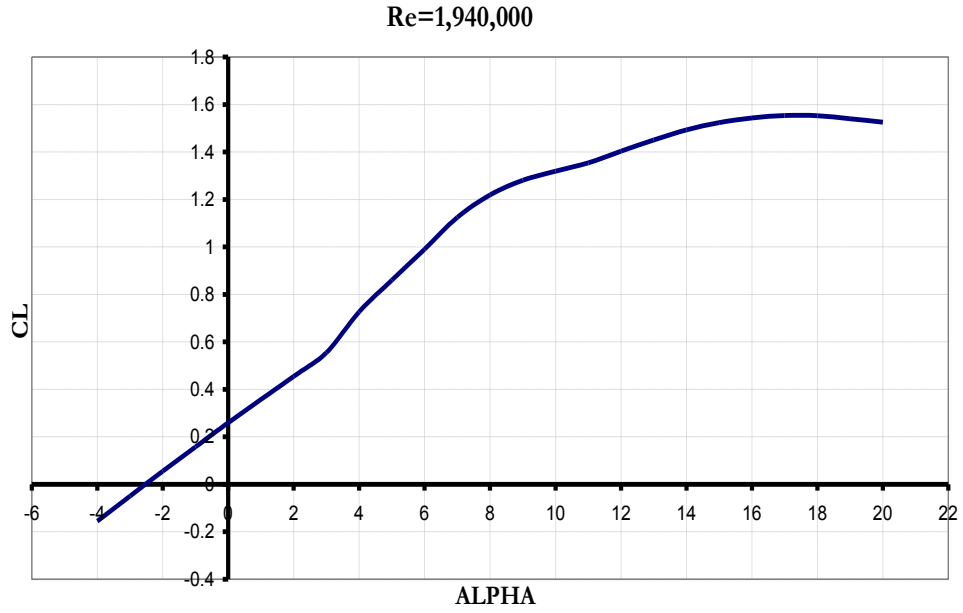

Figure 45: C_L-α Curve Computed for Original KR-2 Stall Speed

[21] Roskam, Jan. Airplane Design, Part VI. Chapter 8. Lawrence, 1990.

Similar plots are obtained for several wing sections.

Chord Length (in)	48	42	36
Chord Length (m)	1.22	1.07	0.91
Re for Stall	1,940,000	1,700,000	1,450,000
Xfoil CL,MAX	1.492	1.476	1.456

Figure 46: $C_{L,MAX}$ for Wing Sections for Stall Calculation

A series of wing lift distributions is now plotted for different α's against the section $C_{L,\,MAX}$ curve. Since the local $C_{L,\,MAX}$ does not vary much across the wing, it is approximated that the relation to chord length is linear. A tabulation of the data used in the plot follows.

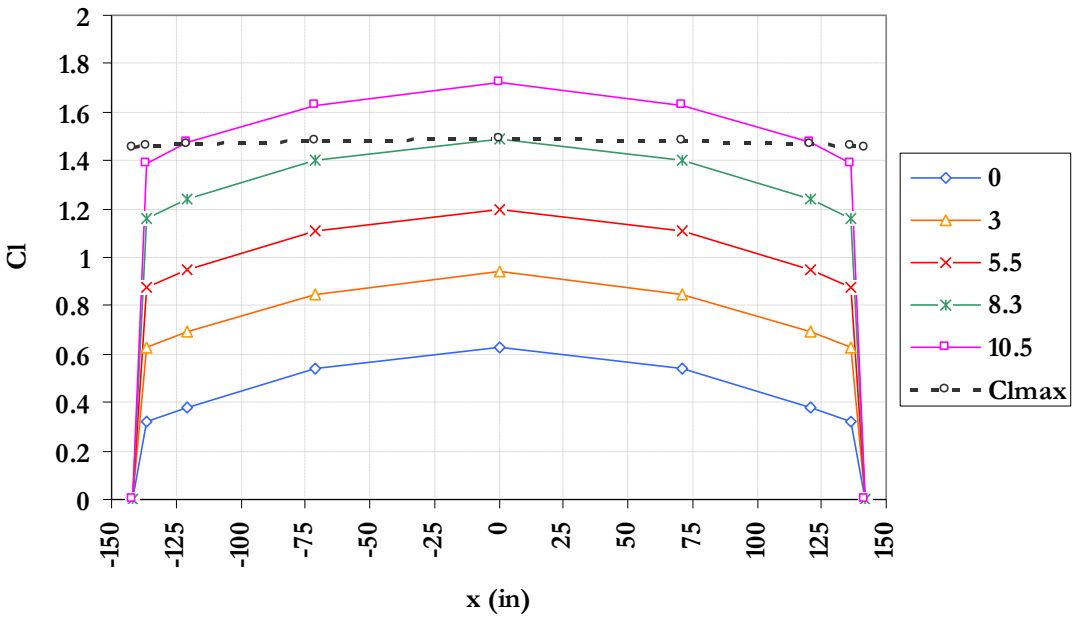

Figure 47: Local Lift Coefficient Distribution for Varying Angle of Attack vs. Local Maximum Lift Coefficient

			α,AIRPLANE→	0	3	5.5	8.3	8.5	10.5	
Wing Station			root α,GEOMETRIC→	3.5	6.5	9.0	11.8	12.0	14.0	
x/s	s(in)	c,0(in)				-----	CL	-----		$CL_{,MAX}$
1.00	-142.0	36.00		0	0	0	0	0	0	1.456
0.96	-136.3	36.77		0.324	0.627	0.879	1.162	1.182	1.384	1.459
0.85	-120.7	38.64		0.381	0.693	0.952	1.243	1.263	1.471	1.464
0.50	-71.0	44.60		0.537	0.850	1.110	1.402	1.423	1.631	1.482
0.00	0.0	48.00		0.625	0.939	1.200	**1.492**	1.513	1.722	**1.492**
0.50	71.0	44.60		0.537	0.850	1.110	1.402	1.423	1.631	1.482
0.85	120.7	38.64		0.381	0.693	0.952	1.243	1.263	1.471	1.464
0.96	136.3	36.77		0.324	0.627	0.879	1.162	1.182	1.384	1.459
1.00	142.0	36.00		0	0	0	0	0	0	1.456
			CLw	0.514	0.821	1.077	**1.366**	1.385	1.589	
			CDi	0.014	0.037	0.065	0.107	0.110	0.146	

Table 3: C_L Distribution for Varying α vs. Local $C_{L,MAX}$; Wing Lift and Wing Induced Drag

At an airplane angle of attack of 8.3°, the lift coefficient curve crosses the $C_{L,MAX}$ curve. This is the point at which the airplane will begin to stall. As seen in Figure 47, the stall begins at the wing root. This is desirable since the ailerons are outboard, and control can be maintained at the onset of the stall. Following the yellow highlights in Table 3 shows that at the onset of stall, the lift coefficient of the entire wing is 1.36. This will serve as the $C_{L,MAX}$ of the wing. Note that the value is less than that of the airfoil due to the downwash for a finite wing.

$$C_{L,MAX,W} = 1.36$$

A new stall speed V_{STALL} can now be calculated with the new $C_{L,MAX}$ of the wing:

$$V_{STALL} = \sqrt{\frac{2W}{\rho_\infty S C_{L,MAX,W}}}$$

$$V_{STALL} = \sqrt{\frac{2(4224\ N)}{(1.225\ \text{kg/m}^3)(8.03\ m^2)(1.36)}} \qquad \textbf{Equation 23}$$

$$V_{STALL} = 25.2\ \text{m/s}$$

$$V_{STALL} = 56.4\ \text{mph}$$

This process can be iterated to more precisely find V_{STALL} by plugging the new value into Equation 21 and redoing this process. However, the low sensitivity of C_L to Reynolds number indicates that such iteration would only yield a change in V_{STALL} by 1-2 mph.

A lift curve can now be created for the wing after determining the zero lift angle of attack, $\alpha_{CL=0,W}$, and the lift curve slope, m_W, from the *Wing Lift Distribution* Matlab program:

$$\alpha_{CL=0,W} = -1.53^o$$

$$m_W = 5.86\ \text{rad}^{-1}$$

$$C_{L,\alpha=0,W} = 0.15$$

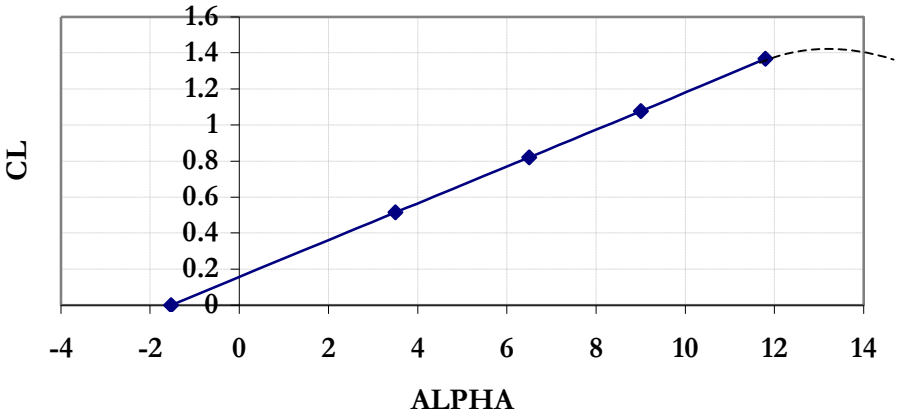

Figure 48: Wing Lift Curve (dashed line is estimation of non-linear region)

IX. Airplane Lift and Drag

A. Airplane Class II Drag Polar Estimation

Now that the wing performance has been calculated, a lift and drag polar for the airplane will be determined. Methodology used here is Jan Roskam's Class II drag polar estimation.[22] Many parameters are retrieved from charts in the Roskam series of airplane design books, and others are calculated here. Hence, a proper review of this next section requires the reader to have the Roskam books on hand in order to review figures. However, all symbols used are defined within this section so that the reader can follow. The lift and drag parameters are tabulated as a function of velocity from 5 to 100 m/s (up to 224 mph) to create the drag polar and other performance numbers. Since many parameters found from reference charts are a function of Mach number or Reynolds number (in other words, a function of velocity), an interpolation has been made to obtain the values of these parameters by running spline interpolation scripts in *Matlab*.

First, the drag on the aircraft is determined. The general definition of drag, *D*, is shown in Equation 24.

$$D = C_D \bar{q} S = C_D \frac{1}{2} \rho_\infty V_\infty^2 S \qquad \textbf{Equation 24}$$

where C_D is the drag coefficient, $\bar{q}$ is the dynamic pressure, and S is the wing planform area. Dynamic pressure is a function of air density, ρ_∞, and airspeed, V_∞, as shown.

The drag is broken down into components for the modified KR-2. Each component of drag is determined. Components include the wing, fuselage, empennage, landing gear, canopy, and miscellaneous components.

$$C_D = C_{D_{WING}} + C_{D_{FUSELAGE}} + C_{D_{EMPENNAGE}} + C_{D_{LANDING\ GEAR}} + C_{D_{CANOPY}} + C_{D_{MISC}}$$

Equation 25

[22] Roskam, Jan. Airplane Design, Part VI. Chapter 8. Lawrence, 1990.

$C_{D_{WING}}$: Wing Drag Coefficient Prediction

The wing drag coefficient is the sum of the zero-lift drag coefficient, $C_{D_{0_W}}$, and the drag coefficient due to lift, $C_{D_{L_W}}$.

$$C_{D_{WING}} = C_{D_{0_W}} + C_{D_{L_W}} \qquad \textbf{Equation 26}$$

For subsonic flow, the zero-lift drag coefficient, $C_{D_{0_W}}$, is computed with:

$$C_{D_{0_W}} = R_{wf} R_{LS} c_{f_w} \left\{1 + L'(t/c) + 100(t/c)^4\right\} S_{wet_w} / S \qquad \textbf{Equation 27}$$

where:

- R_{wf} is the wing/fuselage interference factor. $R_{wf} = 1.075$ from *Roskam VI*[23] Figure 4.1.
- R_{LS} is the lifting surface correction factor. $R_{LS} = 1.07$ from *Roskam VI* Figure 4.2.
- c_{f_W} is the turbulent flat plate friction coefficient. c_{f_W} is a function of Mach and Reynolds numbers, and therefore leads to an interpolation of *Roskam VI* Figure 4.3. Figure 49 below shows the values for which c_{f_W} was calculated (the four data points plotted) and the spline curve from which values will be taken for use in the Class II drag polar tabulation.

[23] Roskam, Jan. Airplane Design, Part VI. Lawrence, 1990. Note: Throughout this chapter, figures, tables, and equations will be referred to from this Roskam's text, in which case, italics '*Roskam VI*' prefacing the item will serve as the reference.

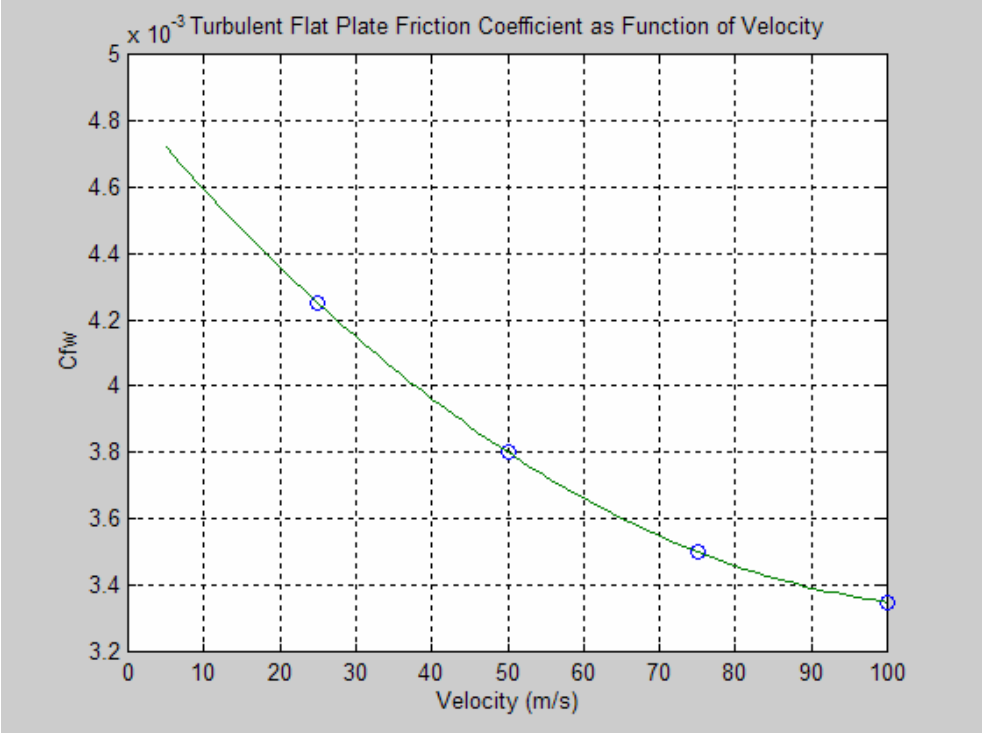

Figure 49: Turbulent Flat Plate Friction Coefficient as Function of Velocity

- L' is the airfoil thickness location parameter. $L'=1.2$ per *Roskam VI* Figure 4.4.
- t/c is the wing thickness ratio. t/c = 0.150 from the airfoil.
- S_{wet_W} is the wetted area of the wing. From *Roskam VI* Appendix B,

$$S_{wet_W} = 2S\left\{1+0.25\left(t/c\right)_r \frac{1+(t/c)_{tip}/(t/c)_{root}\,\lambda}{1+\lambda}\right\}$$

with wing area, S, of $8.03\ \text{m}^2$ and constant thickness ratio, t/c:

$$S_{wet_W} = 2(8.03\ \text{m}^2)\left\{1+0.25\left(.150\right)\right\}$$

$$S_{wet_W} = 16.66\ \text{m}^2$$

$C_{D_{0_W}}$ is tabulated as a function of velocity with these values.

The wing drag coefficient due to lift, $C_{D_{L_W}}$, is computed as:

$$C_{D_{L_W}} = \left(C_{L_W}\right)^2 / \pi Ae + 2\pi C_{L_W}\varepsilon_t v + 4\pi^2 / \left(\varepsilon_t\right)^2 W \qquad \textbf{Equation 28}$$

where the wing lift coefficient, C_{L_W}, is estimated as 5% greater than the coefficient of lift of the entire airplane:

$$C_{L_W} = 1.05 C_L$$

and

- C_L is the coefficient of lift for the entire aircraft.

  $C_L = W / \left(\bar{q}S\right)$ and hence will vary with velocity in the tabulation.

- $A = 6.47$, the wing aspect ratio.
- e is the span efficiency factor.

  $$e = 1.1\left(C_{L_{\alpha_W}} / A\right) / \left\{R\left(C_{L_{\alpha_W}} / A\right) + (1-R)\pi\right\}$$

  where

  - $C_{L_{\alpha_W}}$ is the lift curve slope of the wing, 5.86 rad^{-1} determined from Figure 48.
  - R is the leading edge suction parameter. R is a function of many parameters per *Roskam VI* Figure 4.7.

    $$R = f\left(l_{LER},\ \Lambda_{LE},\ M, A,\ \lambda\right)$$

    Leading edge radius $l_{LER} = 0.0195$ m from *Xfoil* is normalized for mean geometric chord, M (Mach number) is a function of V_∞, and the other wing parameters are calculated in the Chapter V, Configuration.

  $$\frac{A\lambda}{\cos\Lambda_{LE}} = \frac{6.47 \times 0.698}{\cos(0.027\text{rad})} = 4.51$$

  From *Roskam VI* Figure 4.7, $R = 0.96$. Now we calculate e:

  $$e = 1.1(5.86/6.47) / \left\{0.96(5.86/6.47) + (1-0.96)\pi\right\}$$

  $$e = 1.001$$

- ε_T is the wing twist angle, -3.0° or .0524 radians.

- v is the induced drag factor due to linear twist. From *Roskam VI* Figure 4.9, $v = 0.0008$.
- w is the zero-lift drag factor due to linear twist. From *Roskam VI* Figure 4.10, $w = .002$ and varies slightly with speed, tabulated accordingly.

$C_{D_{L_W}}$ is tabulated as a function of velocity with these values. The induced and profile drag of the wing has now been accounted for.

$C_{D_{FUSELAGE}}$: Fuselage Drag Coefficient Prediction

The fuselage drag coefficient is the sum of the zero-lift drag coefficient, $C_{D_{0_{FUS}}}$, and the drag coefficient due to lift, $C_{D_{L_{FUS}}}$.

$$C_{D_{FUS}} = C_{D_{0_{FUS}}} + C_{D_{L_{FUS}}}$$ **Equation 29**

For subsonic flow, the zero-lift drag coefficient of the fuselage is computed with:

$$C_{D_{0_{FUS}}} = R_{wf} C_{f_{FUS}} \left\{1 + 60/\left(l_f / d_f\right)^3 + 0.0025\left(l_f / d_f\right)\right\} S_{wet_{FUS}} / S + C_{D_{b_{FUS}}}$$

Equation 30

where:

- R_{wf} is the wing/fuselage interference factor. $R_{wf} = 1.075$ from *Roskam VI* Figure 4.1.
- $C_{f_{FUS}}$ is the turbulent flat plate friction of the fuselage. From *Roskam VI* Figure 4.3, the parameter varies with velocity. A *Matlab* script 'Cff' was written to interpolate the values of $C_{f_{FUS}}$ as shown in Figure 50.

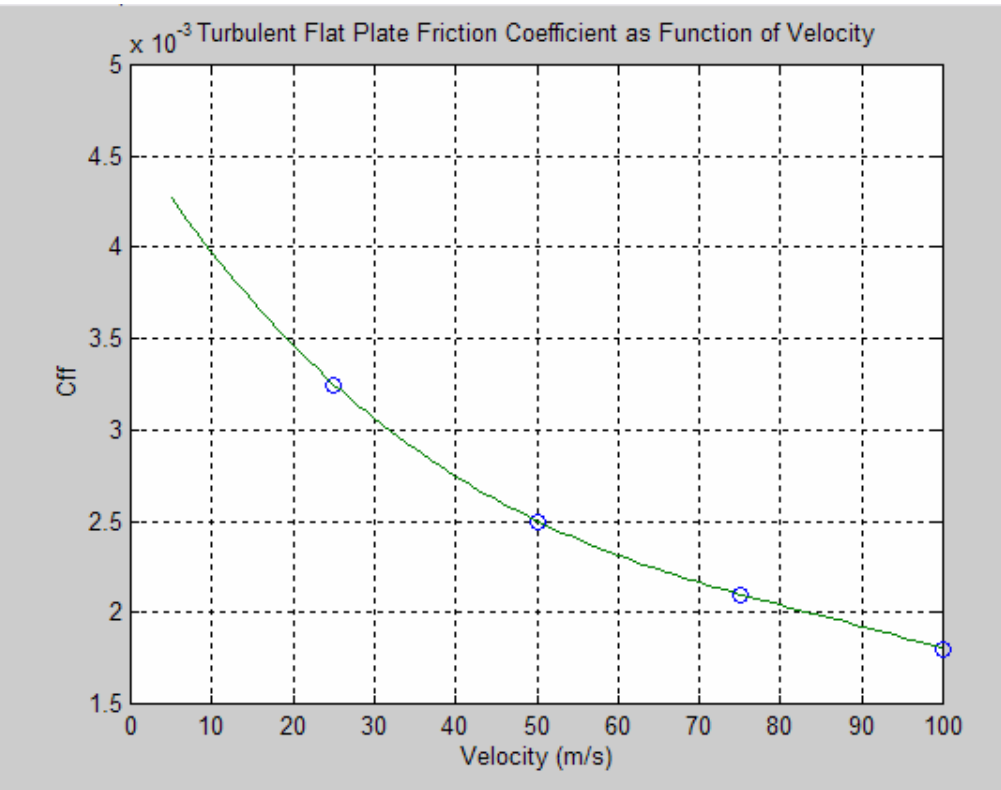

Figure 50: Fuselage Turbulent Flat Plate Friction Coefficient as Function of Velocity

- l_f is the fuselage length. $l_f = 4.42\ \text{m}$.
- d_f is the maximum fuselage diameter. From geometry:

  $$d_f = \sqrt{\frac{4}{\pi} S_{FUS}}$$

  $$d_f = 1.048\ \text{m}$$
- $S_{wet_{FUS}}$ is the wetted area of the fuselage. From *Roskam VI* Figure 4.17

  $S_{wet_{FUS}} = 7.90\ \text{m}^2$.
- $C_{D_{b_{FUS}}}$ is the fuselage base drag coefficient. From *Roskam VI* Figure 4.17

  $C_{D_{b_{FUS}}} = 0$ since there fuselage has no base.

$C_{D_{0_{FUS}}}$ is tabulated as a function of velocity with these values.

The fuselage drag due to lift, $C_{D_{L_{FUS}}}$, is found with the equation:

$$C_{D_{L_{FUS}}} = \eta c_{d_c} |\alpha|^3 S_{plf_{FUS}} / S \qquad \textbf{Equation 31}$$

where:

- η is the ratio of the drag of a finite cylinder to the drag of an infinite cylinder. From *Roskam VI* Figure 4.19, $\eta = 0.61$.
- c_{d_c} is the experimental steady state cross-flow drag. From *Roskam VI* Figure 4.20, $c_{d_c} = 1.2$.
- $S_{plf_{FUS}}$ is the fuselage planform area. From *Roskam VI* Figure 4.17,

  $S_{plf_{FUS}} = 2.92\ \text{m}$.

$C_{D_{L_{FUS}}}$ is tabulated as a function of velocity with these values. The induced and profile drag of the fuselage has now been accounted for.

$C_{D_{EMPENNAGE}}$: Empennage Drag Coefficient Prediction

The empennage drag coefficients are calculated using the same equations as the wing drag coefficients. The profile drag coefficients are calculated for the horizontal stabilizer and for the vertical stabilizer.

The horizontal stabilizer zero-lift drag coefficient is found from:

$$C_{D_{0_h}} = R_{LS} c_{f_h} \left\{1 + L'(t/c) + 100(t/c)^4\right\} S_{wet_h} / S_h \qquad \textbf{Equation 32}$$

where:

- $R_{LS} = 1.07$ per *Roskam VI* Figure 4.2.
- C_{f_h} is interpolated with *Matlab* and *Roskam VI* Figure 4.3 as a function of velocity as shown in Figure 51.

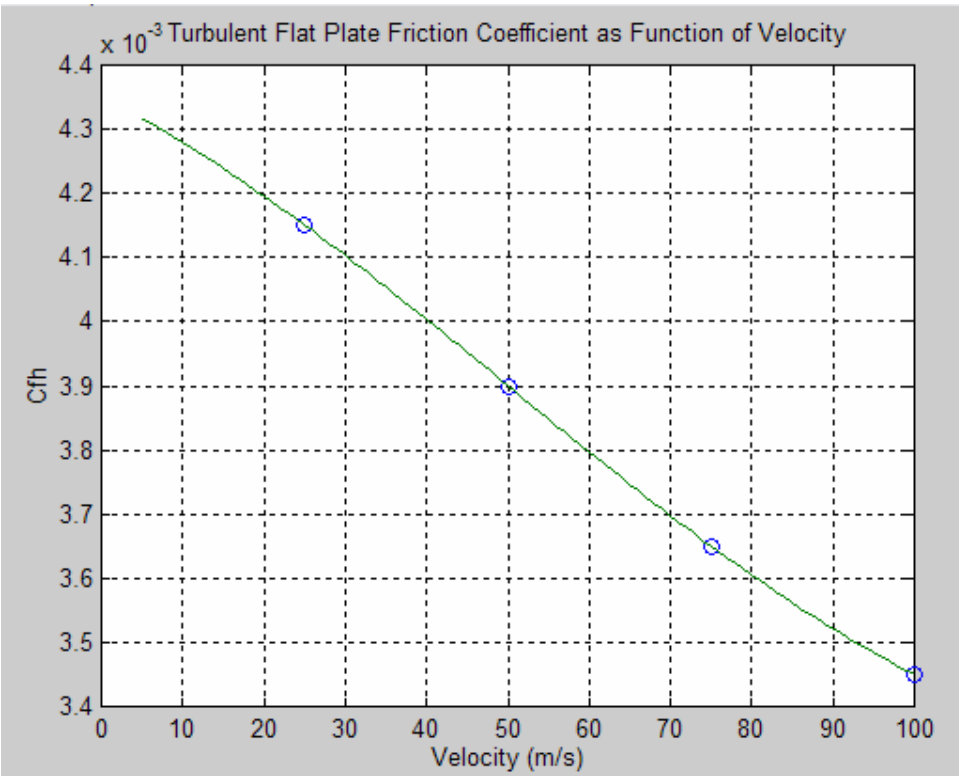

Figure 51: Horizontal Stabilizer Turbulent Flat Plate Friction Coefficient

- $L' = 2.0$ from *Roskam VI* Figure 4.4.
- t/c = 0.0652 from geometry.
- $S_{wet_h} / S_h = 2.1$.

The vertical stabilizer parasite drag is tabulated in the same manner as the horizontal stabilizer and is tabulated accordingly.

The drag of the landing gear is calculated as follows:

$$C_{D_{GEAR}} = \sum C_{D_{GEAR_{CL=0}}} S_{GEAR} / S \qquad \textbf{Equation 33}$$

where:

- $C_{D_{GEAR_{CL=0}}} = 0.565$ from *Roskam VI* Figure 4.54.
- $S_{GEAR} = 0.0267 \text{ m}^2$ from the cross sectional area of the tires.

Hence, for the two landing struts:

$$C_{D_{GEAR}} = 2(0.565)(0.0267)/8.03$$
$$C_{D_{GEAR}} = 0.00376$$

The drag coefficients for the aircraft have been calculated and tabulated for a range of speeds. The drag of the aircraft is then computed from $D = C_D \bar{q} S$. For level un-accelerated flight, thrust is equal to drag, and hence the formula for power is:

$$\text{Power} = \text{Drag} \times \text{Velocity}$$
$$P = DV \qquad \textbf{Equation 34}$$

The P here is referred to as power required (to overcome the drag), but our engine shaft brake horsepower, bhp, is reduced by propeller efficiency, η, to obtain power required. We use a typical propeller efficiency of 0.85 for our hand crafted wooden propeller. Now bhp is computed as:

$$bhp = P_R / \eta \qquad \textbf{Equation 35}$$

Now all columns for the Class II drag polar over the range of speeds is complete. Since the engine is rated at 85 brake HP, the total power available is 85 x 0.85 = 72 HP.

B. Tabulation

All drag and lift parameters are tabulated by velocity up to 100 m/s for a density altitude of 6000 feet. The tabulation as created in Excel is too large to show in its entirety. However, some columns were hidden so that the table may be shown here in acceptable detail:

Velocity	Airplane angle of attack	Airplane lift coef	Wing zero lift drag coef	Wing lift coef	Wing induced drag coef	Wing drag coef	Fuselage zero lift drag coef	Fuselage drag coef due to lift	Fuselage drag coef	horiz. tail zero lift drag coef	Total drag coef	= Cl / Cd	Drag	Power Required	Shaft brake horse power
V	alpha	Cl	Cdow	Clw	Cdlw	Cdw	Cdof	Cdlf	Cdf	Cdoh	Cd_total	Glide Ratio	Drag	Power Required	bhp
mi / hr	deg	n/a	n/a	n/a	n/a	n/a	n/a	n/a	n/a	n/a	n/a	n/a	N	HP	HP
55.9	16.8	1.865	0.012	1.958	0.189	0.202	0.007	0.007	0.013	0.011	0.240	7.8	614	21	24
58.2	15.4	1.724	0.012	1.810	0.162	0.174	0.007	0.005	0.012	0.011	0.211	8.2	584	20	24
60.4	14.2	1.5				151	0.006	0.004	0.011	0.011	0.187	8.6	558	20	24
62.6	13.1	1.4				133	0.006	0.003	0.010	0.010	0.167	8.9	536	20	24
64.9	12.1	1.3	0.012	1.453	0.105	0.117	0.006	0.002	0.009	0.010	0.150	9.2	518	20	24
67.1	11.2	1.295	0.012	1.360	0.091	0.104	0.006	0.002	0.008	0.010	0.136	9.5	503	20	24
69.3	10.4	1.213	0.012	1.273	0.080	0.092	0.006	0.002	0.008	0.010	0.125	9.7	491	20	24
71.6	9.7	1.138	0.012	1.195	0.071	0.083	0.006	0.001	0.007	0.010	0.115	9.9	481	21	24
73.8	9.0	1.070	0.012	1.124	0.063	0.075	0.006	0.001	0.007	0.010	0.106	10.1	474	21	25
76.1	8.4	1.008	0.012	1.059	0.056	0.068	0.006	0.001	0.007	0.010	0.099	10.2	468	21	25
78.3	7.8	0.951	0.012	0.999	0.050	0.061	0.006	0.001	0.007	0.010	0.092	10.3	464	22	26
80.5	7.3	0.899	0.012	0.944	0.044	0.056	0.006	0.001	0.006	0.010	0.087	10.4	461	22	26
82.8	6.9	0.851	0.012	0.894	0.040	0.052	0.006	0.000	0.006	0.010	0.082	10.4	460	23	27
85.0	6.4	0.807	0.012	0.847	0.036	0.047	0.006	0.000	0.006	0.010	0.078	10.4	460	23	28
87.2	6.0	0.766	0.012	0.805	0.032	0.044	0.006	0.000	0.006	0.010	0.074	10.3	462	24	28
89.5	5.7	0.728	0.012	0.765	0.029	0.041	0.006	0.000	0.006	0.010	0.071	10.3	464	25	29
91.7	5.3	0.693	0.012	0.728	0.026	0.038	0.006	0.000	0.006	0.010	0.068	10.2	467	26	30
94.0	5.0	0.661	0.012	0.694	0.024	0.036	0.006	0.000	0.006	0.010	0.065	10.1	472	27	31
96.2	4.7	0.630	0.011	0.662	0.022	0.033	0.005	0.000	0.006	0.010	0.063	10.0	477	27	32
98.4	4.4	0.602	0.011	0.632	0.020	0.031	0.005	0.000	0.006	0.010	0.061	9.9	483	28	34
100.7	4.2	0.576	0.011	0.604	0.018	0.030	0.005	0.000	0.005	0.010	0.059	9.8	490	30	35
102.9	3.9	0.551	0.011	0.578	0.017	0.028	0.005	0.000	0.005	0.010	0.057	9.6	497	31	36
105.1	3.7	0.528	0.011	0.554	0.015	0.027	0.005	0.000	0.005	0.010	0.056	9.5	505	32	37
107.4	3.5	0.506	0.011	0.531	0.014	0.025	0.005	0.000	0.005	0.010	0.054	9.3	514	33	39
109.6	3.3	0.485	0.011	0.510	0.013	0.024	0.005	0.000	0.005	0.010	0.053	9.1	523	34	40
111.9	3.1	0.466	0.011	0.489	0.012	0.023	0.005	0.000	0.005	0.010	0.052	9.0	533	36	42
114.1	2.9	0.448	0.011	0.470	0.011	0.022	0.005	0.000	0.005	0.010	0.051	8.8	543	37	44
116.3	2.7	0.431	0.011	0.453	0.010	0.021	0.005	0.000	0.005	0.010	0.050	8.6	554	39	45
118.6	2.6	0.415	0.011	0.436	0.010	0.021	0.005	0.000	0.005	0.010	0.049	8.4	565	40	47
120.8	2.4	0.400	0.011	0.420	0.009	0.020	0.005	0.000	0.005	0.010	0.048	8.3	577	42	49
123.0	2.3	0.385	0.011	0.405	0.008	0.019	0.005	0.000	0.005	0.010	0.048	8.1	589	43	51
125.3	2.2	0.372	0.011	0.390	0.008	0.019	0.005	0.000	0.005	0.010	0.047	7.9	602	45	53
127.5	2.0	0.359	0.011	0.377	0.007	0.018	0.005	0.000	0.005	0.010	0.046	7.8	615	47	55
129.7	1.9	0.346	0.011	0.364	0.007	0.018	0.005	0.000	0.005	0.010	0.046	7.6	629	49	58
132.0	1.8	0.335	0.011	0.352	0.006	0.017	0.005	0.000	0.005	0.010	0.045	7.4	643	51	60
134.2	1.7	0.324	0.011	0.340	0.006	0.017	0.005	0.000	0.005	0.010	0.045	7.3	657	53	**62**
136.5	1.6	0.313	0.011	0.329	0.006	0.016	0.005	0.000	0.005	0.010	0.044	7.1	671	55	65
138.7	1.5	0.303					0.005	0.000	0.005	0.010	0.044	7.0	686	57	67
140.9	1.4	0.294					0.005	0.000	0.005	0.010	0.043	6.8	702	59	70
143.2	1.3	0.285					0.005	0.000	0.005	0.010	0.043	6.7	717	62	72
145.4	1.2	0.276	0.011	0.290	0.004	0.015	0.005	0.000	0.005	0.010	0.042	6.5	733	64	75
147.6	1.1	0.268	0.011	0.281	0.004	0.015	0.005	0.000	0.005	0.010	0.042	6.4	750	66	78
149.9	1.1	0.260	0.011	0.273	0.004	0.014	0.005	0.000	0.005	0.009	0.042	6.2	766	69	81
152.1	1.0	0.252	0.010	0.265	0.004	0.014	0.004	0.000	0.004	0.009	0.041	6.1	783	71	**84**
154.4	0.9	0.245	0.010	0.257	0.004	0.014	0.004	0.000	0.004	0.009	0.041	6.0	801	74	87
156.6	0.9	0.238					0.004	0.000	0.004	0.009	0.041	5.8	818	77	90
158.8	0.8	0.231					0.004	0.000	0.004	0.009	0.040	5.7	836	80	94
161.1	0.7	0.225					0.004	0.000	0.004	0.009	0.040	5.6	854	82	97
163.3	0.7	0.219	0.010	0.230	0.003	0.013	0.004	0.000	0.004	0.009	0.040	5.5	872	85	100

Stall speed of 56 mph

Cruise speed at 63 bhp

Maximum speed at 85 bhp

Table 4: Tabulation of Class II Drag Polar for Modified KR-2

C. Drag Polar

The drag polar (C_L vs. C_D) curve is plotted for the aircraft. Validation was obtained by verifying that the polar matches within reason to the drag polar of a small aircraft as published. From *Roskam VI* page 118, the drag polar for a Cessna 177 is quite similar.

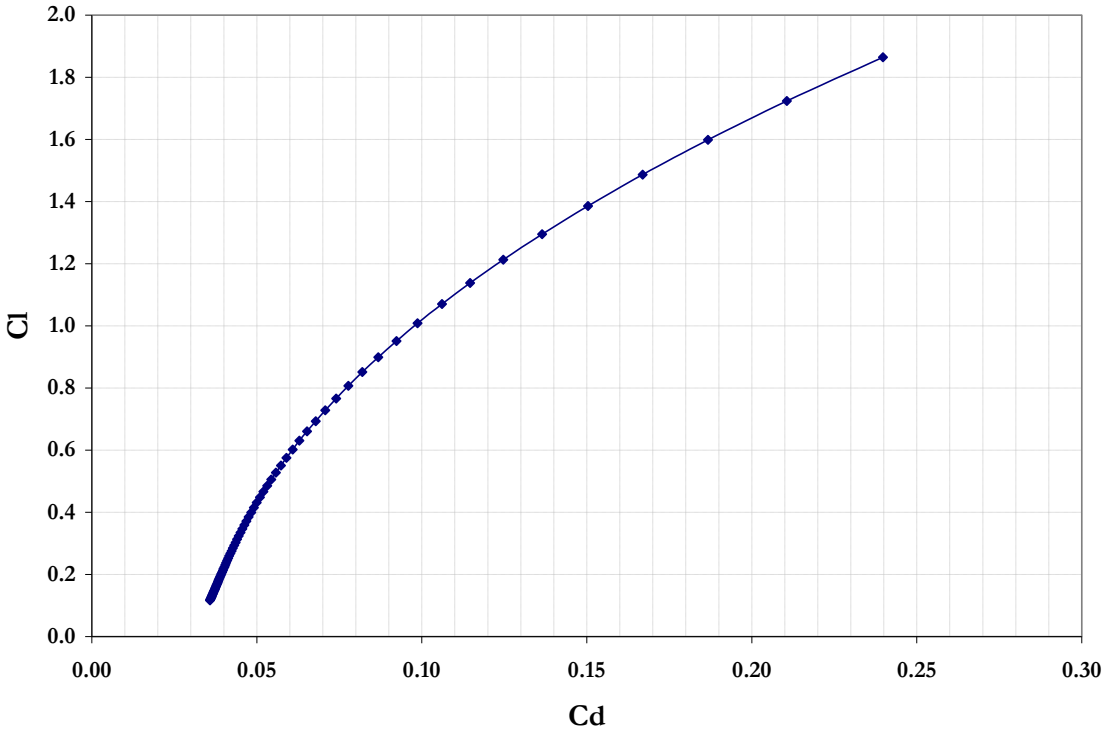

Figure 52: Drag Polar for Modified KR-2 at Gross Weight and at Density Altitude of 6000 Feet

X. Performance

A plot of the power required vs. flight speed reveals the maximum and cruise speeds, and the L/D max, or glide ratio, of 10.4 at 82 mph. Reference Figure 53.

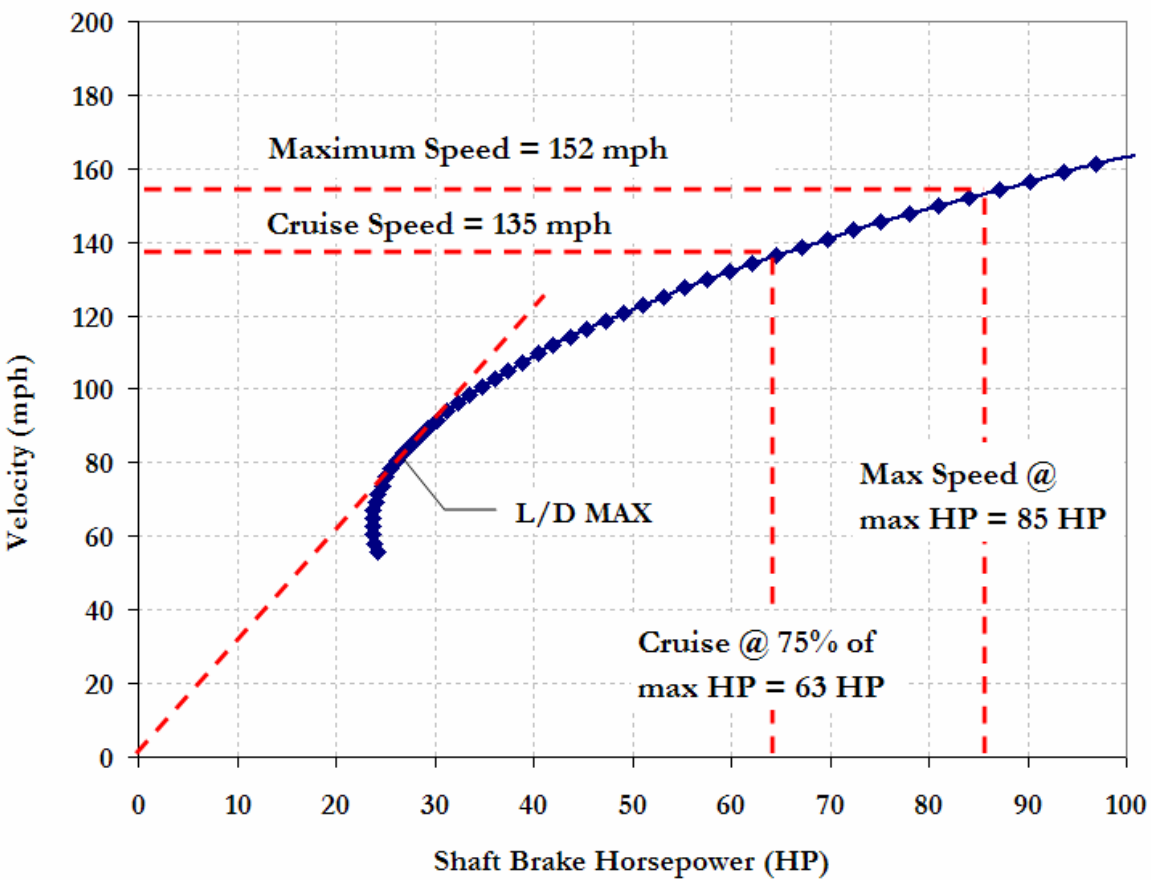

Figure 53: Flight Speed vs. Shaft Brake Horsepower for Gross Weight at 6000 Feet Density Altitude

The climb rate for a given speed is calculated as excess power divided by the weight of the aircraft.

$$R/C = \frac{\text{excess power}}{W} = \frac{P_A - P_R}{W} \qquad \textbf{Equation 36}$$

For a speed of 70 mph the climb rate is about 1500 ft/min, and this decreases to 1000 ft/min at 115 mph.

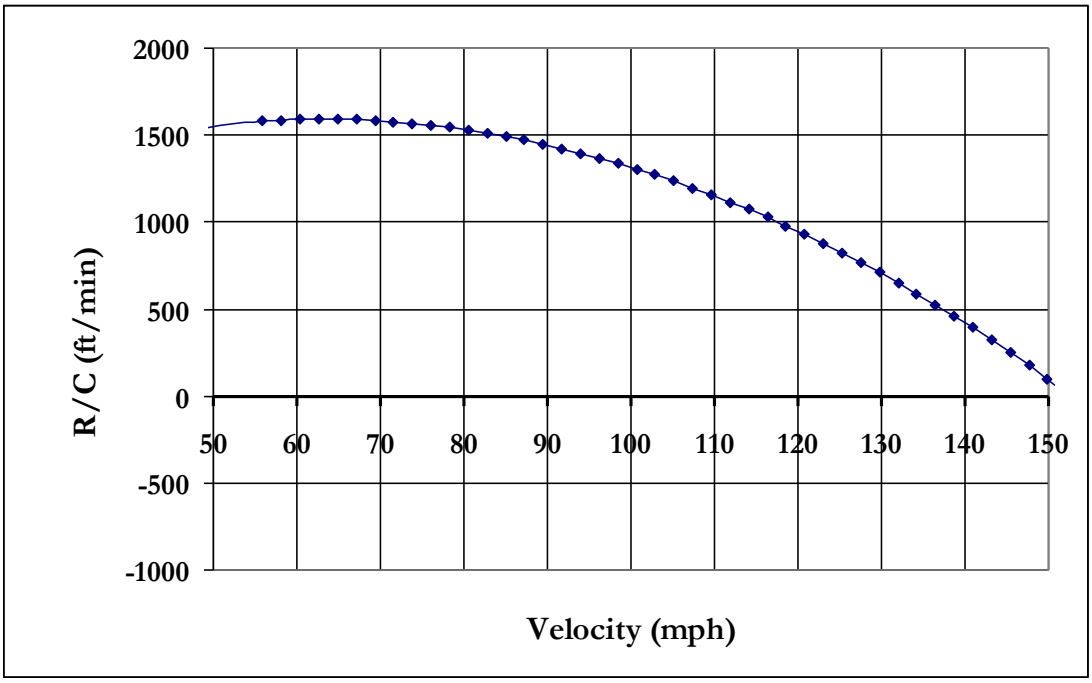

Figure 54: Rate of Climb vs. Velocity, 6000 Ft. Density Altitude

The lift off distance is calculated at 6000 feet, which is approximately the same altitude as the runway at South Lake Tahoe Airport (6260 feet). Calculation is performed at standard atmosphere, for which density, ρ_∞, is 1.021 kg/m^3, and the temperature is 37° F. Assuming the thrust during take off is much larger than the drag and rolling resistance force, the formula for lift off distance s_{LO} is given by Anderson[24] as follows:

$$s_{LO} = \frac{1.44W^2}{g\rho_\infty S C_{L_{MAX}} T} \qquad \textbf{Equation 37}$$

where:

[24] Anderson, John. Introduction to Flight. p. 310.

- $W = 4777\ \text{N}$ (take-off weight)
- $g = 9.81\ \text{m/s}^2$ (acceleration due to gravity)
- $\rho_\infty = 1.021\ \text{kg/m}^3$ (air density at 6000 feet elevation)
- $S = 8.03\ \text{m}^2$ (wing area)
- $C_{L_{MAX}} = 1.36$ (maximum lift coefficient for the aircraft, computed)
- $T = 1512\ \text{N}$ (static thrust available for C-85 engine as tested)[25]

$$s_{LO} = \frac{1.44(4777)^2}{9.81(1.021)(8.03)(1.36)(1512)}$$

$$s_{LO} = 199\ \text{m} = 653\ \text{ft}$$

The published take off distance for the KR-2 is 350 feet at sea level and for a much lighter gross weight than our configuration. It seems reasonable that the take off distance would be nearly double for the added weight at high altitude. Since the runway at the South Lake Tahoe airport is 8,544 feet long, and a good climb rate of 1500 feet was calculated, there should be no problem taking off at gross weight from South Lake Tahoe. As seen from the above equation, and assuming that thrust is proportional to ρ_∞, then it follows that lift off distance is highly dependent on air density:

$$s_{LO} \propto 1/\rho_\infty{}^2$$

Therefore, additional calculations should be made if attempting to fly on a particularly hot day, for which the air density is much lower.

[25] Thrust Testing. http://www.flycorvair.com/thrustjune.html Static thrust measured from test with hydraulic cylinder using a McCauley 71x46 Met-L propeller.

XI. Conclusion

The modified KR-2 has been studied to determine the location of the center of gravity as designed. It is recommended that the most aft loading position is avoided in order to maintain a greater static margin. This can be done by assuring that fuel is always emptied from the wing tanks before the front tank.

A detailed lift analysis of both the airfoil and the wing configuration chosen for this aircraft has been performed. The results of the derivation of the lift distribution obtained with the trailing vortices theory match the results obtained from the computational fluid dynamics within 6%. This is a good validation of the derivation. A quick look at an alternate airfoil shows that the higher $C_{L,MAX}$ may be a good choice to reduce stall speed, reduce take off distance, and improve maneuvering performance.

The lift off distance estimation indicates that take off from Lake Tahoe Airport should be safe at gross weight. However, the cruise speed calculated is 15-20% lower than that for other builders' KR-2s with similar engine size. An effort should be made to reduce the weight of the aircraft and to reduce drag where possible.

Furthermore, the study of the accident reports from the National Transportation Board indicates that it is crucial to have extensive training in the make and model of the experimental aircraft that a builder intends to fly to avoid the statistically high accident rate with low flight hours.

A recommendation for further work on the topic of this KR-2 aircraft in construction includes the calculation of other performance numbers as well as a stability and control analysis. In addition, the added weight to the design leads to a need for a structural analysis. FEA of the wing attachment joint would be a good first calculation.

A summary table of specifications as calculated for the modified KR-2 in comparison the original specification follows.

Definition	KR2 Modified	KR2 Original	Dimension
Length	4.42	4.42	m
Wing Span	7.21	6.30	m
Wing Area	8.03	7.25	m^2
Wing Loading	11.0	11.5	lb/ft^2
Power Loading	11.2	13.9	lb/HP
Aspect Ratio	6.47	5.50	
Mean Geometric Chord	1.113	1.146	m
Fuselage Width	39.0	32.5	in
Empty Weight	552	480	lb
Gross Weight	1073	900	lb
Baggage Capacity	33	35	lb
Take Off Distance	199 at 6000 ft	107	m
Stall Speed	56.4	52	mph
Maximum Speed	152	200	mph
Cruise Speed	135	180	mph
Rate of Climb (gross)	1500	800	fpm
Engine	C-85	VW 2100	---
Engine Weight	204	163	---
Power, Maximum	85	65	HP
Fuel Capacity	28.7	12-35	gal
Fuel Consumption		3.8	gph
Landing Gear	Fixed	Retractable	---
Seating	Two Across	Two Across	---

Figure 55: Specification Comparison for Modified and Original KR-2

XII. Appendix

A. Construction Pictures

Figure 56: Seating in the 'Wide' Modified KR-2

The original design was narrower by 6.5 inches. This kit was intended for narrow people.

Figure 57: Baggage Compartment behind Seat

Figure 58: Seat, stick, Rudder Pedals, and Differential Brake Steering Pedals

Figure 59: Horizontal Stabilizer, Ready for Glassing

Figure 60: Outboard Aft Wing Spars

Figure 61: Propeller with Rough Cuts Completed

Figure 62: Inboard Spars, Outer Wing Attachment Flange

B. Other KR-2 Builders' Modifications and Performance Table

Sport Aviation Article	Builder / Pilot	Engine	HP	Landing Gear Configuration	Modifications	Fuel Capacity (gal)	Empty Weight (lb)	Gross Weight (lb)	Take Off Speed (mph)	Climb Speed (mph)	Climb Rate (fpm)	Cruise Speed (mph)	Maximum Speed (mph)	Stall Speed (mph)	Range (mi)	Why KR-2? Ease of Construction	Why KR-2? Cost	Why KR-2? Speed	Years Building
"A Couple of KRs", September 1995, p. 23	Troy Petteway	Revmaster 2100	80	Conventional fixed	Wide roof, wider main gear track, custom wheel pants, no electrical system, bare minimum	14	520	900	58	138	1000	---	178	---	350	x	---	x	---
"A Couple of KRs", September 1995, p. 23	Bobby Muse	Revmaster 2100	80	Tricycle fixed	Removable front fuel tank, reinforced inboard wing top surface for step, pleated upholstry	---	629	---	---	---	---	---	155	---	---	x	---	---	11
"A Couple of KRs", September 1995, p. 23	Steve Alderman	Continental O-200	100	---	---	---	---	---	---	---	---	---	197	---	---	---	---	---	---
"A Couple of KRs", September 1995, p. 23	Martin Roberts	Continental O-200	100	---	---	---	---	---	---	---	---	---	177	---	---	---	---	---	---
"Tom Crawford's KR-2", February 1999, p. 42	Tom Crawford	VW Type 4 2400	68	Tricycle fixed	Dual ignition, premolded parts, mostly stock, removeable front fuel tank	---	638	1000	1000	---	1300	---	170	40	---	x	x	x	2
"Irish KR-2", May 1987, p. 43	Gerry O'Hara	Tayor 1835	60	Conventional retractable	21 inch fuselage stretch, removable front fuel tank, speed-brake, wing tanks, dual controls	---	600	1000	---	---	---	138	162	46	---	---	---	---	4
"Engine Installation in a Sportplane", March 1986, p. 54	Neil Bingham	Limbach	80	---	13.5 inch fuselage stretch	14	539	798	---	---	---	166	186	---	---	---	---	---	---

Table 5: Other KR-2 Builders' Modifications and Performance Table[26]

[26] Oshkosh, *Sport Aviation Magazine*, articles as noted in table

C. *Matlab scripts*

1. Wing Lift Distribution

```
%  Wing Lift Distribution  %
z=zeros(1,7);
phi=zeros(1,7);
c0=zeros(1,7);
%c0 = spanwise chord length
alpha0=zeros(1,7);
%alpha0 = effective angle of attack
mu=zeros(1,7);
SUM=zeros(1,7);
CL=zeros(1,7);
%CL = spanwise lift coefficient
V=zeros(1,4);
K=zeros(1,7);
M=zeros(4,4);
A=zeros(1,4);
b=zeros(7,7);
c=zeros(7,7);
s=142;
%s = half span in inches
area=12447;
%area is total wing area in inches^2
alpha_i=3.5;
%alfa_i is root wing incidence angle
alpha_cl0=-2.5;
%alpha_cl0 is zero lift angle of attack from airfoil
m=0.1047;
%m is the lift curve slope, = 6.0 1/rad = 0.1047 1/deg
x(1)=0*s;
x(2)=.25*s;
x(3)=.5*s;
x(4)=.675*s;
x(5)=.85*s;
x(6)=.905*s;
x(7)=.96*s;
x(8)=1*s;
i=1;
I=1;
while i<=7;
   phi(i)=acos(x(i)/s);
   if x(i)<42.7
      c0(i)=48;
      alpha0(i)=alpha_i-alpha_cl0;
   else
      c0(i)=48-.12*(x(i)-42.7);
      alpha0(i)=alpha_i-.03*(x(i)-42.7)-alpha_cl0;
   %this if-else clause yields chord length and effective
angle of attack for spanwise wing location
   end
   mu(i)=m*c0(i)/(8*s);
   K(i)=m*c0(i)*alpha0(i)/(4*pi*s);
   V(I)=m*c0(i)*alpha0(i)/(4*pi*s);
   j=1;
```

```
    J=1;
    while j<=7
        b(i,j)=sin(j*phi(i));
        c(i,j)=b(i,j)*j/sin(phi(i));
        a(i,j)=b(i,j)+mu(i)*c(i,j);
        M(I,J)=b(i,j)+mu(i)*c(i,j);
        j=j+2;
        J=J+1;
    end
    i=i+2;
    I=I+1;
end
a;
M;
A=inv(M)*V'
i=1;SUMA=0;nn=1;
while i<=7
    j=1;
    n=1;
    while j<=7
        SUM(i)=A(n)*sin(j*phi(i))+SUM(i);
        n=n+1;
        j=j+2;
    end
    CL(i)=4*pi*s/c0(i)*SUM(i);
    SUMA=i*(A(nn))^2+SUMA;
    %SUMA is sum for induced drag calculation
    i=i+2;
    nn=nn+1;
end
CL
%CLw is total CL for wing
CLw=2*pi^2*s^2*A(1)/area
SUMA;
CDi=pi^3*s^2/area*SUMA
```

2. Wing Turbulent Flat Plate Friction Coefficient Interpolation

```
%Wing skin coefficient as function of velocity
v = 25:25:100;
cfw = [.00425 .00380 .00350 .00335];
vi = 5:1:100;
cfwi=interp1(v,cfw,vi,'spline');
plot(v,cfw,'o',vi,cfwi)
title 'Turbulent Flat Plate Friction Coefficient as
Function of Velocity'
xlabel 'Velocity (m/s)'
ylabel 'Cfw'
grid
format long
cfwi'
```

3. Fuselage Turbulent Flat Plate Friction Coefficient Interpolation

```
%Fuselage skin coefficient coefficient as function of
velocity
v = 25:25:100;
cff = [.00325 .00250 .00210 .00180];
vi = 5:1:100;
cffi=interp1(v,cff,vi,'spline');
plot(v,cff,'o',vi,cffi)
title 'Turbulent Flat Plate Friction Coefficient as
Function of Velocity'
xlabel 'Velocity (m/s)'
ylabel 'Cff'
grid
format long
cffi'
```

4. Horizontal Tail Turbulent Flat Plate Friction Coefficient Interpolation

```
%Horizontal Stabilizer skin coefficient coefficient as
function of velocity
v = 25:25:100;
cfh = [.00415 .00390 .00365 .00345];
vi = 5:1:100;
cfhi=interp1(v,cfh,vi,'spline');
plot(v,cfh,'o',vi,cfhi)
title 'Turbulent Flat Plate Friction Coefficient as
Function of Velocity'
xlabel 'Velocity (m/s)'
ylabel 'Cfh'
grid
format long
cfhi'
```

D. *Software Applications Used*

Gambit	Mesh generator for *Fluent*
Fluent	Computational fluid dynamics solver
Xfoil	DOS based airfoil analysis software
Matlab	Algorithm development language
Pro-Engineer Wildfire	Computer aided design software
Acrobat 3D	3D Acrobat creation suite

E. *Acknowledgements*

Boris Bravo	Coaching in aerodynamics, project foundation
Jan Nordin	Construction partner
Nikos Mourtos	Critical review
Jack McInerney	*Fluent* support
Patrick Flynn	*Xfoil* support
Sheldon Templeton	General support

XIII. Bibliography

Abbott, Ira. Theory of Wing Sections Including a Summary of Airfoil Data. Dover Publications, Inc. New York, 1959.

Anderson, John D. Introduction to Flight. McGraw-Hill. New York, 1978.

Anderson, John D. Fundamentals of Aerodynamics. McGraw-Hill. New York, 1991.

Bairstow, Leonard. Applied Aerodynamics, Second Edition. Longmans, Green and Co. London, 1946.

Bingelis, Tony. The Sport Plane Builder, Aircraft Construction Methods. Tony Bingelis. Austin, 1979.

Bingham, Neil. "Engine Installation in a Sportplane." *Sport Aviation* Mar. 1986: 54-59.

Bingham, Roy. "Design Analysis: A Critical Analysis of the KR-2." *Sport Aviation* Jan. 1988: 38-42.

Bravo, Boris. Design of a Training Aircraft. 1997.

Clutton, Eric. Propeller Making for the Amateur. Tullahoma.

Cox, Jack. "A Couple of KR's." *Sport Aviation* Sep. 1995: 23-26.

Cox, Jack. "KR-2S." *Sport Aviation* Jul. 1993: 38-40.

Cox, Jack. "Tom Crawford's KR-2." *Sport Aviation* Feb. 1999: 42-48.

Drela, Mark. XFOIL 6.9 User Guide. http://web.mit.edu/drela/Public/web/xfoil/ 2001.

Glauert, Herman. Elements of Aerofoil and Airscrew Theory. University Press. Cambridge, 1948.

Custom Built Sport Aircraft Handbook, A Guide to Construction Standards for the Amateur Aircraft Builder. Experimental Aircraft Association. Oshkosh, 1986.

Hurt, Hugh H. Aerodynamics for Naval Aviators. The Office of the Chief of Naval Operations, Aviation Training Division, US Navy. Los Angeles, 1960.

Kunc, Richard. "Ready for Action…A Much-Modified KR-1 with a British Accent." *Sport Aviation* Feb. 1990: 19-24.

Lay, David C. Linear Algebra and its Applications. Addison Wesley Longman, Inc. Reading, 1999.

Lowry, John T. Performance of Light Aircraft. American Institute of Aeronautics and Astronautics, Inc. Reston, 1999.

O'Hara, Gerry. "Irish KR-2." *Sport Aviation* May 1987: 43-46.

Overhaul Manual for Continental Motors Corporation Aircraft Engine Models C75, C85, C90, 0-200. Continental Motors Corporation. Elk Grove Village, 1968.

National Transportation Safety Board – Query. http://www.ntsb.gov/ntsb/query.asp Viewed November 24, 2006.

Perkins, Courtland D. Airplane Performance Stability and Control. John Wiley & Sons, Inc. New York, 1949.

Pilot's Weight and Balance Handbook, AC 91-23A. Flight Standards Service, Federal Aviation Administration. Washington, D.C., 1977.

Rand, Ken. Construction Plans for the KR2. Rand Robinson Engineering, Inc. Huntington Beach.

Roberson, John A. Engineering Fluid Mechanics. John Wiley & Sons, Inc. New York, 1997.

Roskam, Jan. Airplane Design, Parts I-VIII. Roskam Aviation and Engineering Corporation. Lawrence, 1990.

Wynne, William. Thrust Testing: Zenair 601, Cessna 120, Cessna 150, Hudson Corvair, Shop Corvair, Corvair Turbo. http://www.flycorvair.com/thrustjune.html. Viewed December 7, 2006.